AMMONIA GAS ADSORPTION ON METAL OXIDE NANOPARTICLES

by

MOHAMMAD HASAN ABID URF TURABE ALI

B.Tech., Pondicherry University, India, 2006

A THESIS

Submitted in partial fulfillment of the requirements for the degree

MASTER OF SCIENCE

Department of Mechanical and Nuclear Engineering
College of Engineering

KANSAS STATE UNIVERSITY
Manhattan, Kansas

2011

Approved by:

Major Professor
STEVEN J ECKELS

Copyright

Abstract

NanoActive™ metal oxide particles have the ability to destructively adsorb organophosphorus compounds and chlorocarbons. These nanomaterials with unique surface morphologies are subjected to separate, low concentrations of gaseous ammonia in air. NanoActive™ materials based on magnesium oxide have large specific surface areas and defective sites that enhance surface reactivity and consequently improved adsorptivity. In gas contaminant removal by adsorption, presence of vast specific surface area is essential for effective gas-solid interaction to take place. This is also the case in many industrial and chemical applications such as purification of gases, separation and recovery of gases, catalysis etc,. Typically carbonaceous compounds are utilized and engineered in toxic gas control systems. The purpose of this study was to compare NanoActive™ materials with carbon based compounds in the effectivity of toxic gas adsorption at low concentrations.

A test facility was designed to investigate the adsorption properties of novel materials such as adorption capacity and adsorption rate. Adsorption capacity along with adsorption kinetics is a function of properties of the adsorbent and the adsorbate as well as experimental conditions. Nanomaterials were placed on a silica matrix and tested with increasing flow rates. Electrochemical sensing devices were placed at inlet and outlet of the facility to monitor real time continuous concentration profiles. Breakthrough curves were obtained from the packed bed column experiments and saturation limits of adsorbents were measured. Adsorption rates were obtained from the breakthrough curves using modified Wheeler-Jonas equation. The NanoActive™ materials adsorbed ammonia though to a lesser extent than the Norit® compounds.

This study also included measurement of pressure drop in packed beds. This information is useful in estimating energy losses in packed bed reactors. Brauner Emmet Teller tests were carried out for the calculation of surface area, pore volume and pore size of materials. These calculations suggest surface area alone had no notable influence on adsorption capacity and adsorption rates. This lead to the conclusion that adsorption was insignificant cause of absence of functional groups with affinity towards ammonia. In brief, adsorption of ammonia is possible on NanoActive™ materials. However functional groups such as oxy-flouro compounds should be doped with novel materials to enhance the surface interactions.

Table of Contents

List of Figures

List of Tables

Acknowledgements

I bow my head to the Almighty for providing me this good opportunity, to inculcate my thoughts for preparing this thesis which may guide to my successor students in this department of Mechanical and Nuclear Engineering.

I express my deepest gratitude to Dr. Steven J Eckels who has guided in preparing this project by sparing his valuable time. Special thanks to Dr. Ronaldo G Maghirang and Dr. Larry E Erickson who have taken utmost interest in giving stellate suggestions for this work.

I thank all the staff and students at Institute for Environmental Research for all their cordial affection over the time I worked on this research.

I thank my parents, family, friends and specifically my brother Dr.MHU Turabe Fazil M.Sc., (PhD.,), Banaras Hindu University, India, who gave me outstanding moral support whenever needed.

Once again thanking my preceptor and principal man Dr. Steven J Eckels. Praying the Lord to provide all the best to all the persons expressed and implied in completing this comprehensive component.

Dedication

I dedicate this work to the Almighty the creator, the controller, the cognizant and the conspicuous

Nomenclature

A_1 Area above the breakthrough curve from t = 0 to t = t'

A_2 Area below the breakthrough curve from t = 0 to t = t'

A_3 Area above the breakthrough curve from t = t' to t = ∞

B atomic repulsion constant

BET Brunauer-Emmett-Teller

BJH Bopp-Jancso-Heinzinger

BTC Breakthrough curve

C_i Concentration of ammonia gas at the packed bed inlet

C_o Concentration of ammonia gas at the packed bed exit

C_L atomic dispersion constant

d_P granule diameter

e_g effectiveness factor with respect to adsorbate (gas phase)

e_R effectiveness factor with respect to adsorbent (solid phase)

F average field intensity

F_P friction factor

F_{max} maximum intensity above the surface of the solid plane

F_{min} minimum intensity above the surface of the solid plane

k_v Pseudo first order adsorption rate constant

M Molecular weight of the gas/vapors

P_e molar polarization of the adsorbate

Q flow rate

q_o Solute concentration on the adsorbed phase in equilibrium with a concentration C_i in the gas phase

R distance from the surface to the center of charge

r^2 mean square position of all electrons in the molecules with respect to center of charge

Re_P Reynolds number

t_b Breakthrough time in minutes at which the chosen ratio of C_o/C_i appears

VOC Volatile organic compound

W_e Adsorption capacity of the material at a chosen ratio of C_o/C_i

W mass of the adsorbent material in packed bed

ρ_B Bulk density of the packed bed

υ_L superficial velocity

ΔP pressure drop

ε porosity of packed bed or volume fraction

Φ Potential energy of an atom at a distance R from semi-infinite solid

α_1 and α_2 molar polarizabilities of atoms

υ_1 and υ_2 isotropic harmonic oscillating frequencies

Chapter 1 - Introduction

Contaminants often have to be separated from industrial process gases to protect catalysts and indoor air quality (IAQ). According to Environmental Protection Agency (EPA) there are three major reasons for poor IAQ

- Presence of sources that cause indoor air pollution
- Poorly designed ventilation systems
- Use of buildings

Removal of contaminant sources can improve the quality of indoor air environments. Ammonia is one such gas that needs to be maintained at low concentrations for better quality of air. One method of removal is achieved by physical adsorption of gases on filter medium with large internal surface areas. Activated carbon is mainly used in these applications. This research is focused on characterizing the performance of novel 'nano-agglomerated adsorbent materials' subjected to gaseous contamination and their comparison with carbon based compounds.

In this study we report the characterization of nanomaterial based packed bed column for adsorption ammonia in air. The test facility designed to evaluate the nature/characteristics of adsorbents is capable of monitoring real time effects of concentration in the adsorption column. Activated carbon is used to test the *effectiveness* and repeatability of the test system. Differential pressure transducers were used to record the change in pressure drop as a function of volumetric flow rate. Breakthrough analysis predicts life of a given mass of nanomaterial for a specific concentration under standard conditions. Breakthrough curves were obtained using 'Altair-5 multi gas detectors' over time for specific concentrations of contaminants.

Pressure drop- flow rate correlations for packed beds, surface area measurements of specialty materials and breakthrough curve analysis of nanomaterials form the experimental context of this study. Pressure drop-flow rate correlations were obtained to understand the momentum transport in porous media and were compared with the Ergun equation [1]. In order to study the nature of packed-bed system, pressure drop measurements for two uniquely (spherical and pelletized) shaped materials were carried out. BET surface area measurements were performed to calculate the surface area of both commercially available materials and novel nanomaterials to minimize relative error in the estimation of adsorption parameters.

Breakthrough curve analysis of five different materials is presented. Flow variable and mass variable breakthrough curves were investigated. The major purpose of breakthrough curve investigation was to determine the potential sorption characteristics of novel nanomaterials compared to commercially available adsorbents.

Utilizing nanotechnology to improve the efficiency of contaminant removal has the potential to reduce the overall energy requirements of the control volume (more specifically the filter bed). Tailoring the surface chemistry of the filter medium is a crucial step in the effective removal of gas contaminants. There is a need to explore this new and exciting domain of nanotechnology, which has proven to have promising applications. Though there have been public concerns over the adverse effects of these materials, extensive research still needs to be done in the evaluation of nano-materials to address their ultimate use in commercial applications.

Any process that tends to decrease the free surface energy occurs spontaneously. The gas adsorbed by the solid saturates some of the unbalanced forces of the surface, therby decreasing the surface tension. Thus all adsorption phenomenon are spontaneous and result in the decrease of the free energy of the system. Solids have surface tension similar to liquids. Sorption of materials is the direct effect of interaction of atomic forces to relieve this surface tension. When two immiscible solid-gas phases get in contact, usually the concentration of the gas at the interface is greater than its concentration away from the surface. This occurs as the molecules of the gas attached to the surface of the solid partially neutralize the attractive forces of the solid surface, and at equilibrium, the latter acquires its minimum value for the given thermodynamic state of the gas-solid system. This phenomenon is adsorption. Depending upon the nature of binding between the atoms the adsorption is either physical or chemical or both.

This research is primarily focused on evaluation of the performance characteristics of NanoActive™ MgO based particles against a common compound ammonia and comparison with Norit® carbon based materials on their effectiveness in retention of gases. Previous research at KSU developed metal oxide based novel nano-materials with unique surface properties. NanoActive™ MgO based nanomaterials produced had more irregularities or surface defects that offered more reaction sites [2]. One of the interesting properties of NanoActive™ MgO is that it destructively adsorbs certain bacteria and IAQ pathogens and contaminants which make it a promising contender in filtration systems.

Porous materials facilitate an effective interaction between gas and solid phase molecules, due to their vast surfaces available for contact. In fact, with high specific surface areas the probability of interaction of gas molecules goes higher. Also, if the temperatures fall below critical temperature of the adsorbate, capillary condensation will increase the adsorption capacity for a change in phase.

The aim of this research was to explore the merits of applied nanotechnology in removal of gaseous contaminants in indoor air quality. This investigation consists of:

- A systematic approach involving characterization of pressure drop versus flow rate
- Development of test facility to investigate service life for a given amount of packed bed material exposed to ammonia, and
- Comparison of the adsorption capacities and adsorption kinetics of novel materials with Norit® carbon compounds

This thesis is organized into 6 chapters with references and bibliography. Introduction chapter explains the problem statement and overview in general. Background contains a detailed description of fundamental research done previously on physical adsorption and advances in nanotechnology in relative material applications. The Materials chapter discusses some of the synthesis methods employed in the preparation of novel materials. Fourth chapter is the Experimental Facility developed in order to evaluate the adsorption characteristics of novel materials. Detailed explanation of each component is described in this chapter. Results obtained from the breakthrough test facility, BET testing and pressure drop measurements are presented in the fifth chapter. The final chapter presents the conclusion and recommendations from the research.

Chapter 2 - Background

2.1 Introduction

This chapter is focused on the discussion of earlier research directed towards nanoparticle adsorbent systems and work related to effectiveness evaluation of novel materials in adsorption science. NanoActive^{TM} materials have good adsorption characteristics for retention of organophosphorus compounds and chlorocarbons [2]. However, there is no substantial information regarding effectiveness of NanoActive^{TM} materials for the adsorption of low concentration of gaseous ammonia. This review includes information on physical adsorption, adsorption parameters and a brief discussion on earlier research related to physical adsorption and nanomaterials as adsorbents. Section 2.2 focuses on physical adsorption mechanism with emphasis on van der waal forces. Adsorption parameters are discussed with existing models and concept of adsorption equilibrium is reviewed. Nanotechnology review is presented in Section 2.3.

2.2 Physical Adsorption

When gas phase molecules come in contact with a solid phase, a portion is taken up by the solid. The molecules that disappear from the gas phase remain attached to solid surface; this phenomenon is called adsorption. The uptake of charcoal was first discovered by C.W. Scheele in 1773 and by Abbe F. Fontana in 1777. T.Lowitz in 1785 discovered that charcoal took the coloring out by T. de Saussure when he measured the adsorption of variety of gases on several adsorbents [3].

The solid that takes up the gas or vapor is called adsorbent, the gas or vapor attached to the surface of the solid is called adsorbate. As long as the gas does not penetrate into the field of force that exists between the molecules inside the solid, it is considered to be on the outside, even if it is adsorbed on the internal surface area. The site of adsorption is the place where the solid and gas come in contact with each other, i.e., the surface of the adsorbent. The atoms or molecules constituting the solid are held together by different forces: electrostatic or coulomb forces, vander waals forces, etc. The atoms located inside the solid are subjected to equal forces in all directions, whereas an atom on the surface is subjected to unbalanced forces, the resultant

forces inside being greater than the outward forces. This results in a tendency to decrease the surface of the solid (as the forces inside the solid are stronger than the surface forces. Any process that tends to decrease the free surface energy occurs spontaneously. The gas adsorbed by the solid balances some of the unbalanced forces of the surface, therby decreasing the surface tension. Thus all adsorption phenomenona are spontaneous and result in the decrease of the free energy of the system. Adsorption is a surface phenomenon that results in the accumulation of molecules on the surface of the internal pores of adsorbent.

The quantum-mechanical state of the solid and the gas molecule is examined by varying positions and orientations of the molecule relative to the surface. The energy of each state is compared with the energy of the system when the molecule is at a large distance from the surface [4]. In general, the affinity between molecules is due to the difference in the energy among themselves which in turn is created due to the various space derivates of solid phase molecules that would yield the forces and torques on the gas molecule.

Physical adsorption mechanism is a direct consequence due to presence of weak van der waals' forces. According to Brunauer [3], when a molecule reaches the surface of a solid, the electronic interactions among the molecule and solid sometimes keep their respective associations. In some cases the molecule and solid may enter into covalent and ionic bonds, affecting the chemical and electronic properties of both the molecule and the solid. Physical adsorption is usually associated with a small amount of chemical activity and this activity is termed as chemisorption. Inorganic vapors are typically chemisorbed at the energetic sites of the adsorbent surface. In general, the energetic sites in materials have surface deformities due to the excess energy attained during their synthesis process. Certain compounds get entrapped more effectively over others depending on the surface morphology. The volatile compounds in the indoor air come from many sources including building materials, furnishings and occupant activities and in some cases, the ventilation air. Adsorption bed systems designed for odor control and other low contaminant concentration applications (<10 ppm) have filters that are discarded as they approach saturation limits with the contaminant. These systems are termed non-regenerative as the adsorbent is not reused.

2.2.1 Van der waals interaction

Physiosorption is a type of adsorption in which the adsorbate adheres to the surface only through van der waals interactions, which are also responsible for the non-ideal behavior of real gases. Van der waal's forces on a solid surface arise due to London dispersion forces (LDF) [4]. The LDF is a weak intermolecular force resulting when two electrons in adjacent atoms occupy positions that make the atoms form temporary dipoles. An atom or molecule can develop a temporary dipole when its electrons are distributed asymmetrically about the nucleus. The gas molecules possess permanent dipole/multipole moments which can induce attracting charge distributions in the solid and interact with any permanent external field of the solid

- *Pair wise forces between single molecule*

Dispersion forces were first recognized by London [4] between pairs of atoms or molecules. Dispersion forces are weak, long-range interactions which arise due to charge fluctuations in the two interacting atoms. London stated that the quantum-mechanical ground state of an atom the electrons have significant amount of kinetic energy. Therefore the instantaneous charge distribution would possess electric moments even though on the average the distribution might be spherically symmetric. Atoms in their ground state are approximated by simple isotropic harmonic oscillators of frequencies υ_1 and υ_2, London obtained the equation:

$$\boldsymbol{C_L = \frac{3}{2}\alpha_1\alpha_2\frac{h\upsilon_1\upsilon_2}{\upsilon_1+\upsilon_2}} \tag{2.1}$$

where $\alpha_1$and α_2 are the polarizabilities of the atoms.

- *Surface forces by lattice integration*

It is difficult to find an accurate description of the quantum state of the solid. If the repulsive terms are also included, the potential energy $\boldsymbol{\phi}$ of an atom at a distance R from a semi-infinite solid with a uniform density of ρ atoms per unit volume is given by

$$\boldsymbol{\phi(R) = -\frac{\rho\pi}{3}\left(\frac{C}{2R^3}-\frac{B}{15R^9}\right)} \tag{2.2}$$

- *Surface forces treating the solid as a single solid system*

The dispersion interaction between a molecule and a solid should be determined from the appropriate properties of the solid treated as a unit in itself rather than by the use of lattice sums. For interaction of an external molecule with a conduction surface, Lennard-Jones assumed that the instantaneous charge distribution of the molecule induced its classical image in the neighboring conductor [4]. In terms of distance R from the surface to the center of charge, if r^2 is the mean-square position of the electrons, interaction energy is:

$$\boldsymbol{\phi(R) = \frac{-e^2\langle r^2\rangle}{12R^3}} \tag{2.3}$$

- *Electrostatic forces*

For ionic crystals an external classical electric field is described by an electric field intensity F. This field will induce a dipole or higher order moment in the charge distribution of an admolecule which is attractive. The admolecule may have a permanent electric dipole or quadrapole moment which can also interact with F. The average field intensity is calculated from the expression

$$\boldsymbol{F^2 = \frac{1}{2}\left(F_{max}{}^2 + F_{min}{}^2\right)} \tag{2.4}$$

where F_{max} and F_{min} are the maximum and minimum intensities above the surface.

The most sophisticated formulation was that of Lenel to attempt to allow for the rapid spatial variation of F. If P_o is the potential at the center of adatom and P the potential at other points in the atom, potential can be expressed ϕ as:

$$\boldsymbol{\phi = \int \frac{(P - P_o)\rho\, dv}{\Delta}} \tag{2.5}$$

Where ρ is the atomic electron density, $\Delta$is a characteristic energy of the adatom (atom at the surface) which is about the ionization potential for inert gases and the integration is the volume of the adatom [4]. These potentials represent different atomic forces that cause the van der waal interactions which is the major source of physical adsorption mechanism.

2.2.2 Chemical forces of interaction

When interaction between solid surface and gas results in covalent and/or ionic bond, electronic structures of both adsorbate and adsorbent molecules are rearranged and their initial properties are distorted. Chemical forces at the interface are more intricate than those discussed for van der waals' forces; in addition detailed discussion of chemical nature is out of context so the discussion is limited to listing its classification. Chemical interactions are classified as follows

Surface chemical bond

- Ionic bond
- Covalent bond
- Co-ionic bond

Surface states and chemical forces

2.2.3 Adsorption Capacity and Adsorption Rate

Amount of the adsorbate adsorbed per unit mass of the adsorbent at a given gas-phase concentration under equilibrium conditions is known as adsorption capacity. Adsorption involves mass transfer of adsorptive molecules to the peripheral surface of the adsorbent and then moves into the pores (intragranular diffusion) and the molecule gets adsorbed into the surface. Adsorption therefore is a function of properties of adsorbate and adsorbent and experimental conditions such as volumetric flow rate, temperature and humidity. Physical adsorption is considered to be second order in kinetics, involving the reaction between surface active sites and a gas molecule. The breakthrough curve (BTC) resulting from the effluent concentration profile plotted against time exhibits second order kinetics in the mid-portion of the curve. Measurement of second order rate reactions with two reactants (solid and gas) is difficult. So, it is assumed that the interaction between the gas and solid surface follows pseudo-first order reaction. This assumption is convenient since the measurement and calculation of second order curve reduces precision of rate approximation [5]. The pseudo first order reaction is essentially a second order reaction and the nature of reaction involves one of the reactants to be present in excess amounts such that the effect of the other reactant is negligible. The first portion of the curve, with low concentrations of vapor penetrating the bed, represents excessive active sites over free gas molecules as shown in Figure 2-1. Analogously, the final portion of the curve

represents the portion of the curve, where the number of vacant sites is rapidly being depleted. This represents an excess of gas molecules over active sites.

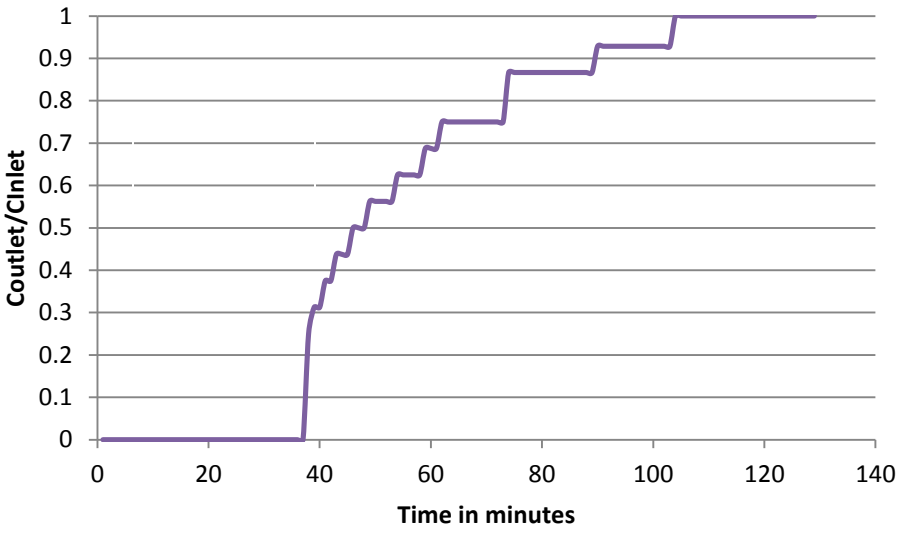

Figure 2-1 Breakthrough curve

EPA describes three important terms used in actual systems for defining capacities of the packed bed [6]. *Breakthrough capacity* is defined as the capacity of the bed at the time where unadsorbed vapor begins to be emitted. *Saturation capacity* (or equilibrium capacity) is the maximum amount of vapor that can be adsorbed per unit mass of adsorbent. This is the capacity read from the adsorption isotherms. *Working capacity* is a fraction of the saturation capacity, often in the range from 0.1 to 0.5 of the saturation capacity that is used for design purposes. Smaller working capacities increase the amount of carbon required. In this study adsorption characteristics below 5% gas penetrations of gas concentrations are characterized by pseudo-first-order-kinetics with respect to gas molecules and working capacities for a fraction of 0.1 relative to the saturation capacity were evaluated.

Wheeler. A and Robell [7] derived kinetic Equation (2.6), applicable to the study of vapor adsorption by beds under dynamic flow conditions, from a continuity equation of mass balance between vapor entering an adsorbent bed and the sum of the vapor adsorbed by plus that penetrating bed. The Wheeler equation can be written as

$$t_b = \left(\frac{W_e}{C_i Q}\right)\left[W - \frac{\rho_B Q\, ln\left(\frac{C_i}{C_o}\right)}{k_v}\right] \tag{2.6}$$

where t_b is the breakthrough time in minutes at which the chosen concentration C_o (g/cm^3) appears in the exit stream, C_i is the inlet concentration(g/cm^3), Q is the volumetric flow rate (cm^3/min), ρ_B is the bulk density of the packed bed (g/cm^3), W is mass of the adsorbent (g), W_e is the adsorption capacity($g_{ammonia}$ /$g_{adsorbent}$) at the arbitrarily chosen ratio of C_o/C_i and k_v is the pseudo first order adsorption rate constant (min^{-1}). Though the equilibrium adsorption capacity is an important parameter, for characterizing predictive performance breakthrough time is more significant [8]. When breakthrough time t_b is plotted versus amount of carbon, it results in a straight line curve, from slope and x-axis intercept the properties of W_e and k_v can be calculated.

2.2.4 Existing models for the Adsorption Rate-Coefficient

Substantial research has been done in development of a method for determining the value of k_v (rate coefficient) from breakthrough curves. Rate coefficient instinctively defines how fast or slow a given interaction takes place. Since k_v cannot be measured directly from experiments, it has to be calculated from the breakthrough time from Equation (2.6). Model development and model comparison is usually based on a standardized method for calculating k_v. Three different methods are discussed below.

Breakthrough time t_b is plotted against amount of material as a variable at fixed C_o/C_i. k_v is obtained from the slope and intercept of the regression line. Large errors will propagate if the extrapolated intercept is close to zero. In addition, the calculated value of k_v is dependent on the breakthrough fraction (C_o/C_i) chosen. k_v is calculated for a breakthrough fraction (C_o/C_i) of 0.1 and using a known value of W_e. A plot of $\ln[(C_i-C_o)/C_o]$ versus time t_b for varying C_o/C_i. The estimation of the second parameter, the overall adsorption rate coefficient k_v, is less straightforward. Initially, some basic estimations were developed, based on theoretical diffusion models. An alternative method was the experimental determination of k_v by means of a single breakthrough experiment [8]. Several authors have proposed semi-empirical Equations for estimation of k_v. The most recent one has been put forward by Lodewyckx and Wood [9] (Eq. 2.7), k_v is derived from the slope and intercept of the regression line. This approach employs the

least-squares method to calculate the line of best fit to multiple points on the breakthrough curve. The random error in the observations is taken into account as part of the regression calculations.

Jonas et al. [8] proposed a model that uses k_v derived according to the method at a 1% breakthrough fraction

$$\boldsymbol{k_v = 111.6 {v_L}^{0.5} {d_p}^{-1.5}} \tag{2.7}$$

where υ_L is the superficial velocity in cm/sec and d_p is the granule diameter in cm. In our experiments 10% breakthrough fraction has been used, hence the above equation should have a different form. Since this model does not account for the influence of properties of the adsorbate, it is not valid in the present context.

Wood [9] suggested a model that is based on a large number of *k* values calculated from experimental breakthrough curves:

$$\boldsymbol{k_v = \left\{ \left[\left(\frac{1}{v_L} \right) + 0.027 \right] * \left[0.000825 + \frac{0.063 - 0.0058 ln \left[\frac{(C_{in} - C_{out})}{C_{out}} \right]}{P_e} \right] \right\}^{-1}} \tag{2.8}$$

where υ_L is the linear velocity in cm/sec, P_e is the molar polarization of the adsorbate (cm^3/mol), C_{in} is the inlet concentration in ppm and C_{out} is the outlet concentration in ppm, Though the influence of the properties of adsorbate on *k* is taken into account through P_e in this equation, the influence of adsorbent in not taken into account.

Equation suggested by Lodewyckx and Vasant [9]:

$$\boldsymbol{k_v = \frac{48 \beta^{0.33} {v_L}^{0.75}}{{d_p}^{1.5}}} \tag{2.9}$$

Value of k_v is calculated at 10% breakthrough fraction using a known adsorption capacity, W_e. The model doesn't take into account the random experimental error introduced by using only one point on the breakthrough curve. The value of k_v is therefore strictly valid only for breakthrough fractions close to 10%.

All these models are not based on the systematic investigation of the parameters that might influence k_v, such as velocity, inlet concentration, nature of adsorbent and adsorbate. A set of experimental data therefore is necessary to know the experimental variation of k_v under the influence of all the variables stated above. The performance of Wheeler Jonas equation for predicting breakthrough times is polished by the investigation of real values of k_v. Adsorption rate constant is a function of temperature, flow rate, adsorbent particle size and molecular weight of the adsorbate gas. For any given adsorbate compound the rate constant in the test facility under study can be predicted with ammonia as reference gas at constant temperature, flow rate and porosity/grain size of packed bed material, from the following correlation [5]

$$\left(k_v M^{\frac{1}{2}}\right)_i = \left(k_v M^{\frac{1}{2}}\right)_{ref} \tag{2.10}$$

Contrary to most organic vapors, an inorganic vapor (ammonia) chemisorbs when it is passed through a carbon filter bed. Physiosorption and chemisorption, have some important differences as stated before. Contrary to the physisorption, the forces in chemisorption are similar to those acting in chemical reactions and such a chemisorption is associated with a reaction heat. Chemisorption is a specific unimolecular reaction, taking place at the active sites of the carbon surface. Therefore, the activated carbon needs to be impregnated with specific complexes. According to Jonas in the case of ammonia, H_3PO_4 or H_2SO_4 are the appropriate impregnants for the best result [11]. Soo-Jin Park et al., [12] produced activated carbon fibers (ACFs) by an oxyfluorination treatment to enhance the capacity of ammonia gas removal. The oxyfluorinated ACFs led to an increase of fluorine and oxygen-containing polar functional groups in ACF surfaces, resulting in an increase in the ammonia-removal efficiency of the ACFs produced. The ammonia-removal efficiency of the ACF's was enhanced by the oxyfluorination, despite the reduction in specific surface areas.

2.2.5 Adsorption Equilibrium

Equilibrium established for a given amount of gas at a given temperature and pressure is a function of the nature of the adsorbent and adsorbate. This includes the size, shape and pore size distribution and chemical constituents of the solid and properties of gas (ammonia). Earliest correlation of adsorption with known physical properties of the adsorbed gases was made in

1814 by de Saussure [4]. Adsorption of molecules occurs only when their potential energy is at a minimum.

The study of the fixed-bed operation must include an estimation of the efficient use of both adsorbate and adsorbent. Figure 2-2 shows the geometric interpretation of the utilization of adsorbate and adsorbent based on the areas of the different zones of a typical breakthrough curve. In order to quantify the performance of the adsorption operation in a fixed bed, several effectiveness factors have been defined in the literature. Effectiveness factors with respect of adsorbate, e_g, and adsorbent, e_R, can be expressed, respectively, as follows [13-14].

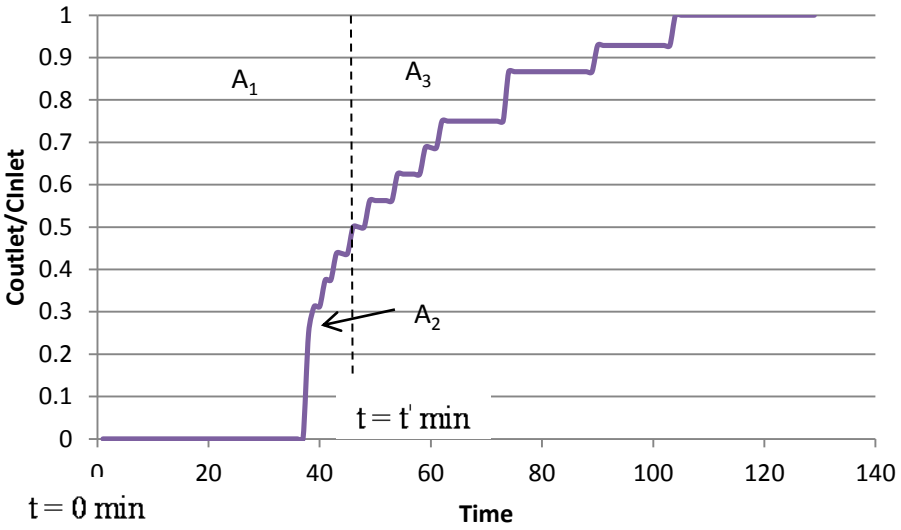

Figure 2-2 Geometric interpretation based on effectiveness factor

$$e_g = \frac{A_1}{A_1 + A_2} \tag{2.11}$$

$$e_R = \frac{A_1}{A_1 + A_3} \tag{2.12}$$

Bautista et al. [15] estimated numerically the effectiveness factor of the adsorbent according to the following equation

$$e_R = A_1 \frac{QC_i}{(q_o.W + \varepsilon_L.V.C_i)} \tag{2.13}$$

Breakthrough curves are significantly asymmetric with respect to the breakthrough point. e_R allows the comparison of the bed efficiency, relative to the corresponding adsorption capacity, at any given experimental conditions in any adsorbate-adsorbent system. It is the ratio of actual amount of adsorbate inside the column to the sum of maximum amount of adsorbate inside the column adsorbed and adsorbate contained inside the bulk liquid phase between particles. In the present work, the effectiveness parameter e_R was calculated for a 10% cutoff, that is, for a *k* value corresponding to a ratio of 10% of outlet to inlet concentration in the column bed. This cutoff value was chosen arbitrarily in order to compare the results between different experiments carried out at different operating conditions.

2.3 Nanotechnology Review

Nanotechnology can be defined as the science that develops materials by manipulating matter at the molecular and atomic level. One nanometer is equal to one-billionth of a meter in size. The scale is so small, that it is often difficult to manipulate at this level. Nanotechnology is also defined as the study of matter within the size range of 10^{-6} to 10^{-9}meters. The term *nano* is a Latin term meaning 10^{-9}. Nano-materials have huge specific surface areas i.e., surface area per unit mass.

Materials that exist at a scale of 10^{-9} meters come under the classification of Nanoscience. They are notable for their extremely small size or grain size and hence have the potential for extensive industrial, chemical, biomedical, and electronic applications. Nanomaterials can be metals, metal oxides, ceramics, polymeric materials, or composite materials. They have a wide range of potential applications from making sensors to chips. One promising application is that of adsorption. The high surface area, ease and cost-effective fabrication of the nanofilters may allow them to compete with ceramic and polymer based separation membranes used commercially. In order to perform various separation applications with nanoscale structures in a practical way, appropriate large-scale structures need to be designed and built with nanoscale units

Depending on the adsorbent and adsorbate, nanoadsorbents can possess advantages over traditional adsorbents in areas that impact adsorption capacity: surface area, pore size distribution, and surface chemistry (Shelly, 2003). One distinguishing characteristic of nanometerscale structures is that, unlike macroscopic materials, they typically have a high

percentage of their constituent atoms at a surface. The volume of an object decreases more quickly than its surface area as the size diminishes. This scaling behavior leads, in the most extreme case, to structures where nearly every atom in the structure is interfacial.

2.3.1 Surface Area in Nanomaterials

Enhanced surface areas ensure enhanced surface reactivity with gas molecules and employs effective phase interactions between the adsorbent and adsorbate. Since there is more surface available for interaction in nanomaterials, amount of matter needed for a given interaction is drastically minimized due to the high specific surface area they possess. This attribute of nanomaterials provide sustainability in usage of materials. As regards to the pore size, it impacts not only the surface, but also access to adsorption sites, i.e. smaller pore sizes may not accommodate larger molecules.

Srivastava et al., [16] reported the fabrication of freestanding monolithic uniform macroscopic hollow cylinders having radially aligned carbon nanotube walls, with diameters and lengths up to several centimeters. Using a continuous spray pyrolysis method they have synthesized macroscale hollow carbon cylinders, with walls (ranging from 300 μm to 500 μm thick) consisting of micrometer length aligned multi walled nanotubes (MWNTs). These Nanostructures were used as filters to demonstrate their utility in two important settings: the elimination of multiple components of heavy hydrocarbons from petroleum a crucial step in post-distillation of crude oil with a single-step filtering process, and the filtration of bacterial contaminants such as *Escherichia coli* or the nanometresized poliovirus (=25nm) from water. The product is however more useful for removal process at small scales and lacks structural integrity in pilot scale applications.

Kalabunde et al., [2] prepared Nanocrystals of MgO and CaO by a modified aerogel drying method. These materials destructively adsorbed organophosphorus compounds. The term "*destructive adsorbent*" is defined as the ability to efficiently adsorb and chemically destroy incoming adsorbate. It is basically dissociative adsorption on a large scale. High surface area and high surface reactivity are desired properties of destructive adsorbents, and nanoparticles fill the need perfectly. Nanoscale MgO and CaO particles exhibit unusual surface morphologies and possess more reactive surfaces due to the presence of high concentrations of edge/corner sites and other defects. Furthermore, at higher temperatures (400-500 °C), these high surface area

materials are effective destructive adsorbents for toxic substances such as organophosphorus compounds and chlorocarbons. These unique materials were chosen to test for adsorption capacities against toxic gas mixtures.

Mangun et al., [17] reported tailoring of the pore surface chemistry of activated carbon fibers as an effective method for increasing the removal efficiencies of various contaminants under a fixed bed configuration. The adsorption kinetics was described by a homogeneous surface diffusion model. This appears to be the first study which constructs a phenomenological model for a fixed bed of activated carbon fibers.

Stephan brosillon et al., [18] reported experimental results of adsorption of volatile organic compounds (VOCs) on zeolite and proposed simulations of the breakthrough curves based on the linear driving force model. A constant value of effective diffusivity is found independent of the nature and the amount of VOCs adsorbed. A relation linking intrapellet mass-transfer coefficient and equilibrium constant is proposed, including the average effective diffusivity, to make predictions of breakthrough curves for any kind of volatile organic pollutant in gaseous effluents.

Chapter 3 - Materials

3.1 Activated Carbon

Activated carbon is solid, black carbonaceous material distinguished from elemental carbon by the absence of both impurities and an oxidized surface. It can be prepared from a large number of sources such as coconut, wood, peat, coal, tar and sawdust. To increase the surface area, the carbon is then "activated" by using steam, air, or carbon dioxide at higher temperatures. These gases attack the carbon and increase the pore structure. The temperatures involved, amount of oxygen present, and type of feedstock all greatly affect the adsorption qualities of the carbon. Activated carbon has large surface area and pore volume, making it suitable for a wide range of applications [5]. It can be used as a decolorizing agent, a taste and odor-removing agent or as a purification agent in food processing. The applications range from water treatment, purification in clothing, textile, automobile, and cosmetics to adsorbent in gas mask filters. Not only is it cheap but also a major adsorbent for a large variety of organic compounds.

The most important property of activated carbon, the property that determines its usage, is the pore structure. The total number of pores, their shape and size determine the adsorption capacity and even the dynamic adsorption rate of the activated carbon. Porous structures are classified relative to their pore diameter or pore width. Macropores are the void zones inside the porous structures that have a diameter > 50nm, mesopores are pores within the range of $2 \leq d \geq 50$nm and micropores are the smallest possible pores < 2nm in diameter.

3.2 NanoActive^{TM} materials

- NanoActive^{TM} MgO

NanoActive^{TM} MgO is an interesting chemical adsorbent. These are large hexagonal platelets with well ordered multilayers. There are different MgO based NanoActive^{TM} materials commercially available from Nanoscale Corporation, Manhattan, Kansas. Since this study is focused on MgO based materials, physical properties of these materials are briefly discussed.

NanoActive^{TM} MgO is a magnesium oxide powder produced by Nanoscale Company. Commercially available MgO is boiled in distilled water with magnetic stirring. After cooling, the slurry is filtered, and the filter cake is dried in an oven at 120 °C. The dried powder was broken into pieces and heat treated to 500 °C under vacuum in a Pyrex reaction tube inside a

cylindrical furnace. The material was heat treated over 12 hours and the sample was maintained at 500 °C. This is labeled as CP-MgO which means conventionally prepared MgO. NanoActive™ materials demonstrate a selection of interesting properties such as enhanced surface reactivity, high surface area and large pore volume. Table 3.1 [19] shows the chemical and physical properties of NanoActive™ MgO. SEM image of NanoActive™ MgO is shown in Figure 3-1 [19]. The basic particle has a volume weighted average size of 16 μm. These are essentially aggregates that formed into clusters of nanoparticles. The building material is around 100 to 300 nm in size.

Table 3-1 Properties of NanoActive™ MgO

Specific Surface Area	≥ 230 m^2/g
Crystallite Size	≤ 8 nm
Average Pore Diameter	50Å
Total Pore Volume	≥ 0.2 cc/g
Bulk Density	0.6 cc/g
True Density	3.2 g/cc
Mean Aggregate size, $d_{0.5}$	3.3 μm
Moisture Content	≤ 1%
Mg Content (Based on Metal)	≥ 95%

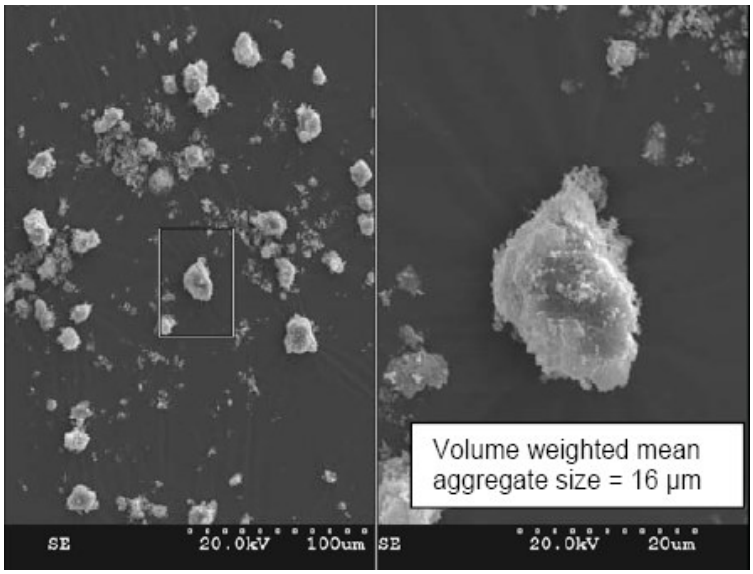

Figure 3-1 SEM image of NanoActive™ MgO

- NanoActive™ MgO-G

NanoActive™-G MgO is basically granular form of NanoActive™ MgO powder with same chemical properties (Figure 3-2). Production of these materials was to further enhance the applicability of NanoActive™ MgO in separation technology. This form is quite useful in applications where there is requirement for a low pressure drop, so these materials are expected to toil for rewarding surface interactions.

- Nanozorb™

Nanozorb is mainly a doped material with Zinc oxide and Titanium dioxide. Since only 30% of NanoActive™ MgO reacts with compounds, research has been done to develop novel materials to provide a better compound in terms of overall efficiency. Magnesium oxide though does not have any hazardous polymerization limitation; it has been declared EPA category 3 for acute eye irritation and EPA category 4 for acute dermal irritation. To minimize the health risks titanium dioxide and zinc oxide is doped and the material transformed into practically non-irritating (acute eye irritation) and non-toxic (acute dermal irritation). Chemical composition is reported as below:

Table 3-2 Chemical Composition of Nanozorb®

Component	OSHA PEL	ACGIH TLV
Magnesium Oxide	15 mg/m^3	10 mg/m^3
Titanium Dioxide	15 mg/m^3	10 mg/m^3
Zinc Oxide	15 mg/m^3	10 mg/m^3

Figure 3-2 commercially available NanoActive™ MgO powder

3.3 Norit Activated Carbon

- Norit RZN01

Norit RZN01 is industrial grade extruded form of activated carbon doped with $ZnSO_4$ specifically manufactured for removal of ammonia. This material consists of 1mm diameter cylindrical pellets.

- Norit RBM 40M

Norit RB 40 M is a steam activated extruded carbon with a diameter of 4mm. It is recommended for applications where carbon bed pressure drop is a major consideration.

- Norit Vapure 410

Norit vapure 410 is commercially available granular activated carbon recommended for use in gaseous applications involving purification and separation processes. It is a premium grade recommended for removal of odors, toxic vapors, irritants, corrosive gases, and to recover

solvents and hydrocarbons from various gas streams. Table 3-3 [20] presents the physical properties and exposure limits of commercially available Norit® compounds.

Table 3-3 Comparison of Norit® compounds

Property	RZN01	RB 40M	Vapure 410
Bulk Density- Granular grades	21-25 lbs/ft^3	21-25 lbs/ft^3	28-34 lbs/ft^3
Bulk Density- Powder grades	15-35 lbs/ft^3	15-35 lbs/ft^3	15-35 lbs/ft^3
Solubility in water	Insoluble	Insoluble	Insoluble
Appearance and odor	Black granules	Black granules or powder with no odor	Black granules or powder with no odor
Respirable Fraction	2.5 mg/m^3	2.5 mg/m^3	3 mg/m^3
Total Dust Exposure limit (TWA 8-hr)	7.5 mg/m^3	7.5 mg/m^3	10 mg/m^3
CCl_4 activity g/100g	n/a	60 min	n/a
Ball-pan hardness	n/a	95 min	95 min
Moisture %	n/a	5	2
Iodine Number mg/g	n/a	900-1000 min	1050 min
Apparent Density lb/ft^3	n/a	32	31

Chapter 4 - Experimental Facility

4.1 Introduction

Removal of contaminants from gas streams is most commonly achieved by packed columns (adsorption). Two different packed bed columns were used in this study. A packed bed facility was set up for the evaluation of HEPA filters embedded with powdered Nanoactive^{TM} MgO; the procedure employed for estimation of adsorption capacity is mass based. A facility with a long column was developed for the estimation of pressure drop across packed beds as a function of flow rates. Another facility was designed for the estimation of adsorption capacity of nanomaterials as adsorbents in packed beds. Setup, operation, usage and calibration of packed bed column test facilities are discussed in this chapter.

By definition a packed bed is a fixed layer of small particles arranged in a vessel to promote intimate contact between gases, vapors, liquids, solids, or various combinations thereof; used in catalysis, ion exchange, sand filtration, distillation, absorption, and mixing. In adsorption, the fixed bed arrangement can either be random or arranged depending upon the application. The purpose of a packed bed is typically to improve contact between two phases. Shape of packing materials has a direct influence on the surface areas and void space between the packing [18]. The chemical reaction takes place on the surface of the adsorbent. Experimental facilities were designed after taking into account the influencing factors of a given set of dependent and independent variables.

4.1.1 Packed bed column1

Characterization of pressure drop versus flow rate was performed in the packed bed column facility. The experimental test facility for packed bed column-1 is schematically illustrated in Figure 4-1. The long cylindrical column is made up of polyvinyl tubing which is supported on a wooden frame along its length. There are two bronze T-joints at the top and bottom of the column to bypass incoming air flow inside the pressure transducers, for the measurement of change in pressure drop at inlet and outlet. The pressure regulator is fitted to automatically cut off the air flow at excessive pressures. This helps in providing a steady flow reducing noise and preventing damage to the facility. Compressed air from the compressor is passed into the packed bed facility through pressure regulator. Flow process is depicted in the block diagram in Figure 4-1.

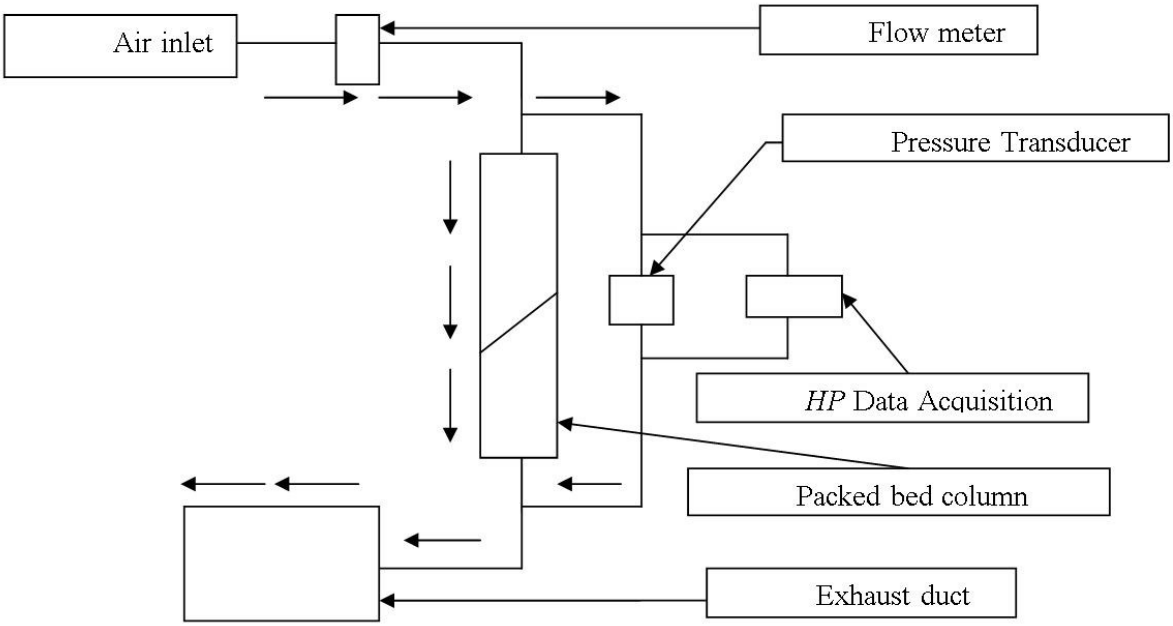

Figure 4-1 Block diagram of Packed bed column-1

Variable area flow meter RMB 51 ssv (Dwyer Inc.) controls the airflow through the pipe line. The diameter of the column is 0.75 inches and the distance between the T-joints is 33.75 inches. Orifices are provided on the column at T-junction brass joints to pass the flow into the differential pressure transducer. The differential pressure is measured by the capacitance step strain gauge where the changes in pressure are converted to DC voltage. The transducer is

connected to a Hewlett Packard 34970A data acquisition unit that communicates using RS-232 protocol and records the pressure drop inside the column. Wire mesh sieves were used at both the ends of the bed in order to avoid loss of material. In addition the wire mesh provides uniform packing at the inlet and outlet of the column and helps minimize randomness in flow patterns.

Cylindrical pellets of activated carbon and spherical zirconium marbles of 5mm diameter were arranged in the test facility (Figure 4-2) and the packed bed was tested for pressure characterization. Compressed air flow is supplied from a compressor attached to a flow meter through a pressure regulator. Volumetric flow rates were varied over a range of 2 to 12 SCFH (Standard Cubic Feet per Hour) and the resultant pressure drop measurements were taken down over the length at 23±1°C.

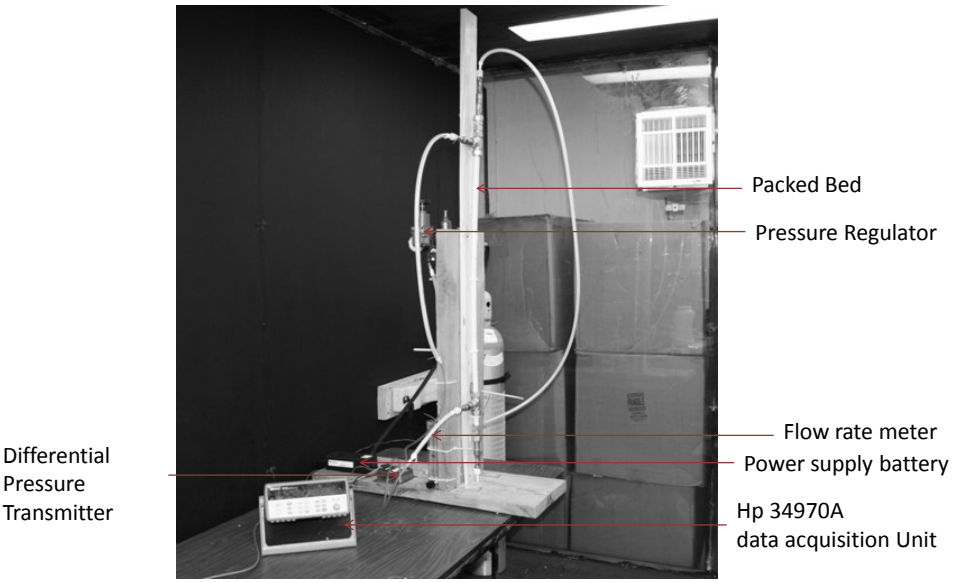

Figure 4-2 Packed bed test facility

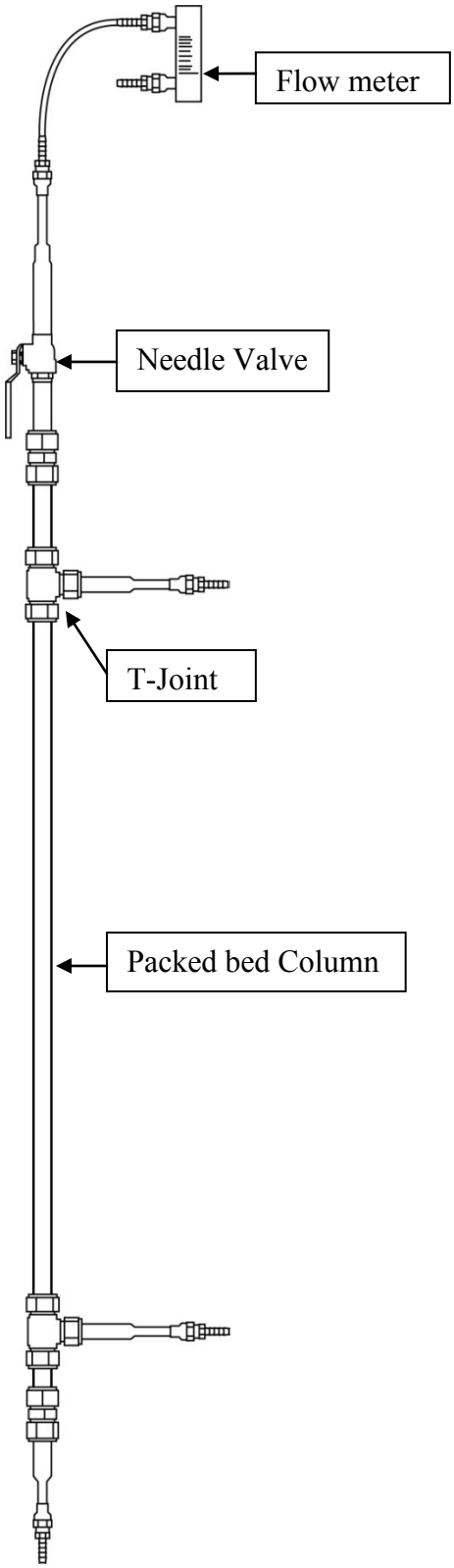

Figure 4-3 Packed bed column-1 test section

4.1.2 Packed bed column2

All breakthrough curve experiments were conducted in the specialty test column manufactured exclusively for Nanomaterial characterization. This is made up of glass and the maximum length of the bed that can be tested is 17mm as shown in Figure 4-3. Tapered glass near the inlet is available for ease in adsorbent loading. A specialty glass fitting helps to disassemble the upper portion of the testing facility and the packing material can be loaded from the top. A silica based matrix with sieves at micro-scale is embedded by glass blowing at the bottom of the column; this facilitates holding the nanomaterials in the packed bed without letting them to pass into the effluent. Diameter of the silica matrix is 19mm and width 4mm. Two component inorganic mixture of ammonia with air commercially available from Matheson-tri gas was setup in the test chamber. The concentration of ammonia used for the experiments is 50 ppm (balance air). High purity single stage pressure regulator is used to provide point-of-use pressure monitoring and control. The ammonia cylinders are connected to the facility in a test chamber and the regulator is installed directly into the gas lines with a single delivery pressure gauge. The pressure gauge is used to monitor the pressure within the gas cylinder. The basic component of a gauge is a hollow metal tube that expands and contracts at exact amount under varying pressures. This tube is connected to a series of gears. These gears are further connected to a needle, which can be viewed on the top of the dial. VFA-3 variable area flow meter is used to control the flow rates of ammonia gas at the inlet of the packed bed. Filter flasks (1000 mL Kimax Kimble specifications in table) were installed into the flow line at the inlet and exit of test column to enable proper mix for sampling of the ammonia gas. If the sampling probes were to be installed directly into the pipe lines, it may cause huge pressure drops and may even cause choking. The filtered flasks provide a volume of 1000mL in between the flow line for continuous sampling without damaging the pipe line. Specifications of filtered flask used are present in Table 4-1. A blower is positioned at the outlet to create negative pressure in the test chamber for preventing ammonia leakage inside the chamber.

Table 4-1 Specification of filtered flask

Item	Capacity (mL)	Graduated Interval (mL)	Subdivision (mL)	Rubber Stopper Size	Approximate Widest Diameter (mm)	Approximate Height (mm)	Case Quantity
27060-1000	1000	300 to 1000	50	8	135	230	12

The practical challenge to hold nanomaterials in a packed bed column arises from the fact that the size of the particles is very small (10^{-9} m). Previous research at KSU produced agglomerates of these nanoparticles that gave rise to clusters of larger scale (10^{-6} m) without losing the properties at nanoscale [2]. However holding micron sized particles in a packed bed and allowing the fluids to pass through them without losses in amount of material is complicated. We introduced a silica based glass matrix that can hold the particles of micron scale range, prepared by glass-blowing at the Chemistry Department of KSU. This allows the nanomaterials to be characterized in a packed bed column without losing the material. The packed bed test column is shown in Figure 4-4. Flow process is shown in block diagram Figure 4-5 with a picture of facility in Figure 4-6.

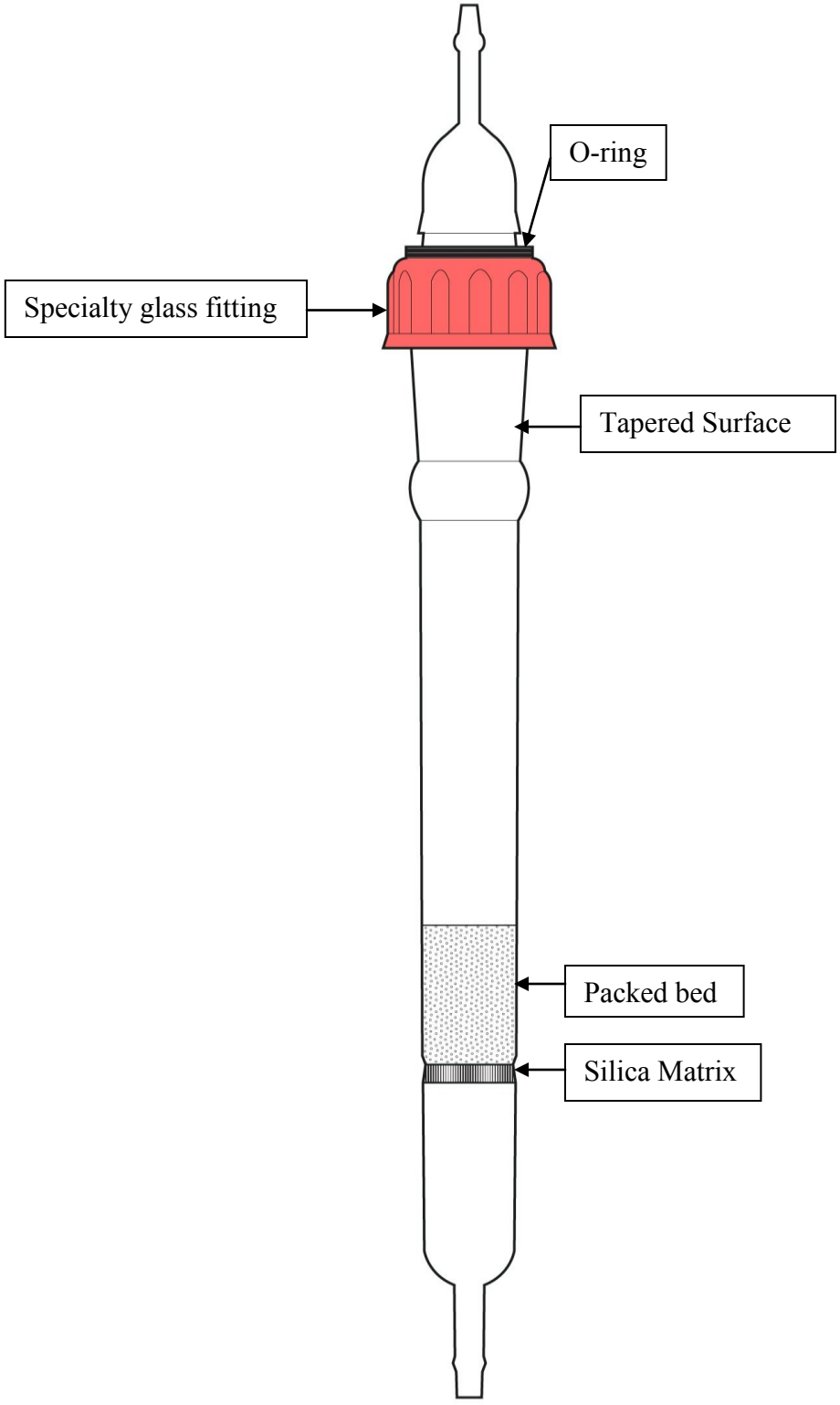

Figure 4-4 Packed bed column-2 test section

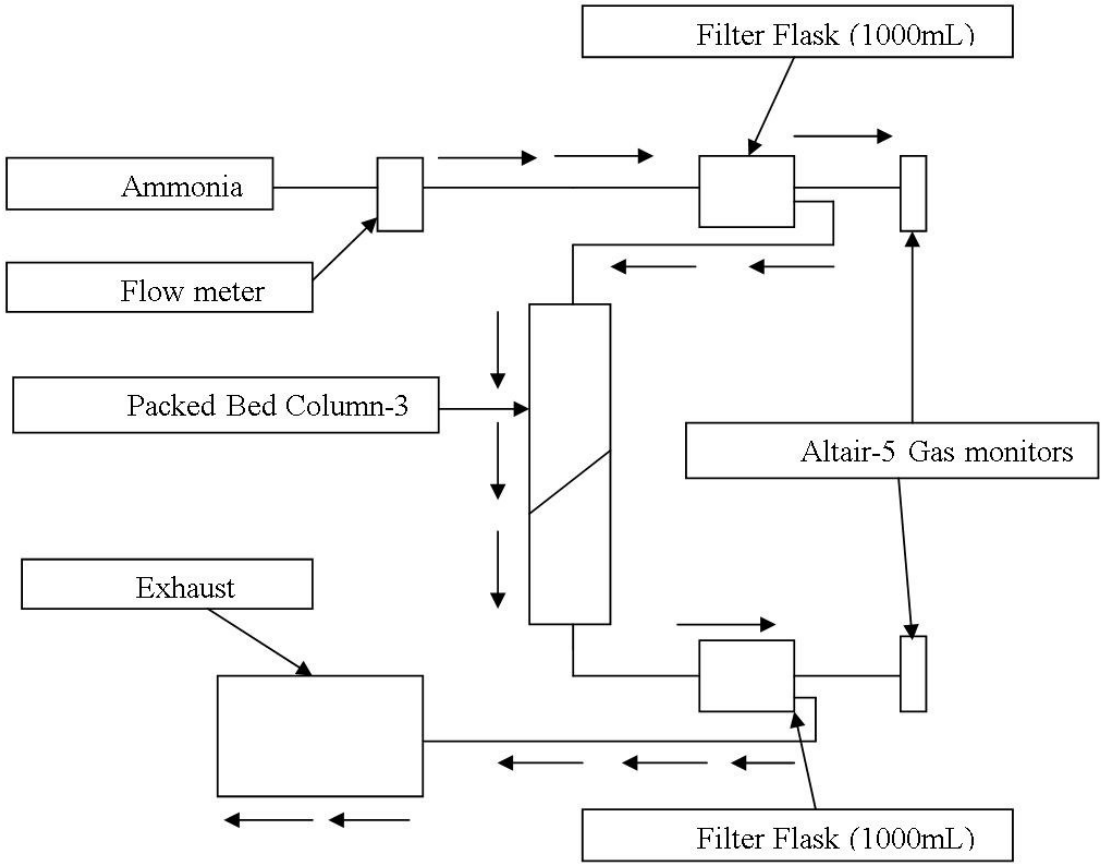

Figure 4-5 Block diagram of packed bed column-2

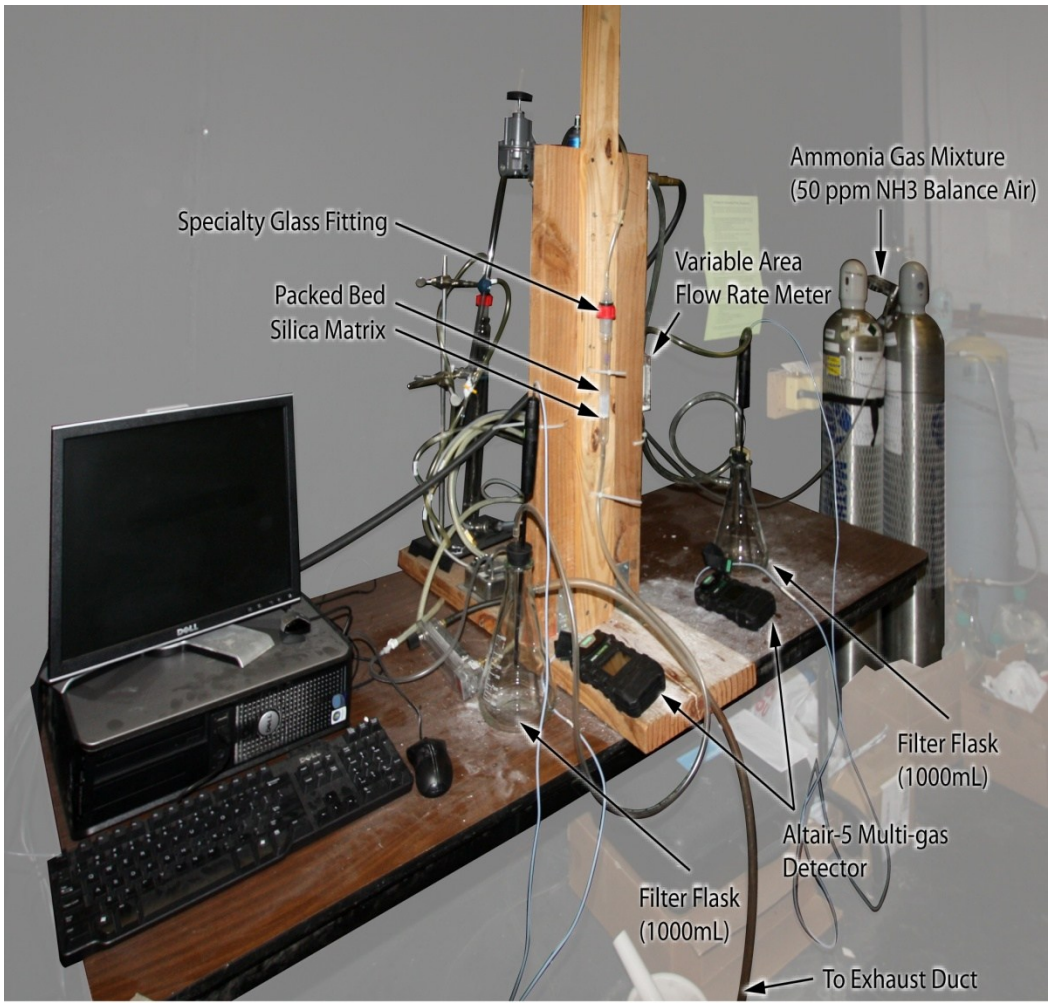

Figure 4-6 Nanomaterial packed bed test facility

4.2 Instrumentation and Measurement

4.2.1 Altairs-5 Multi-gas detection system

Altair-5 multi gas is an electrochemical sensing device employed to monitor gas concentrations at the inlet and outlet of the test facility. Altair-5 is embedded with four sensors as shown in Figure 4-7, which can display readings for 5 separate gases. Electrochemical sensors are basically fuel cells composed of noble metal electrodes in an electrolyte. The electrolyte is an aqueous solution of strong inorganic acids. When a gas is detected the cell generates a small current proportional to the concentration of the gas.

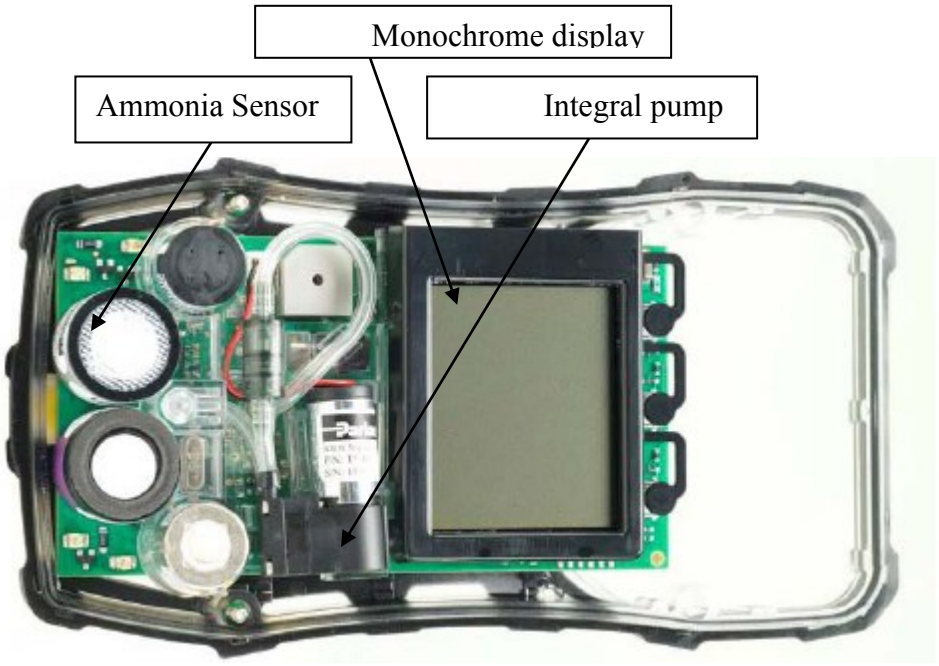

Figure 4-7 Front view of Altair-5 gas monitor

The detector is installed with an integral pump configuration for continuous monitoring. Figure 4-7 shows the inside view of monitor with ammonia sensor and integral pump installations. Though the oxygen sensor is approved for use only up to 21% oxygen, it has the capability to detect up to 25% oxygen in ambient air. STEL (short term exposure limit) alarm and TWA (time weighted average) alarms are configured for ammonia the subject gas under surveillance. The weight of the instrument is 0.45kg with battery and the dimensions are 17 (cm) x 8.87 (cm) x 4.55 (cm). There are two battery types one with rechargeable Li ION battery and replaceable AA alkaline batteries. The monitor run time is 14+ hours at 25°C until the battery wears off. The instruments share the same charging time ≤ 6 hours (maximum safe charging voltage U_m=6.7 Volts D.C.). The operational temperature range for the instruments is around -20°C to 50°C, whereas for instruments with NH_3 sensors the range shifts to -20°C to 40°C. Humidity Range includes 15-90% relative humidity; non-condensing, 5-95% RH intermittent and Atmospheric Pressure range is 80 kPa to 120 kPa.

Measuring methods:

- Combustible gases- catalytic sensor
- Oxygen gas- Electrochemical sensor
- Toxic gases- Electrochemical sensor

The measuring ranges for each sensor embedded inside the monitor are listed in Table 4-2. The concentration range of ammonia is from 0-100 ppm essential to monitor the variations of 50ppm gas.

Table 4-2 Measuring range monitored in Altair-5 Multigas detector

Gas type	H_2S	CO	O_2	Combustible	NH_3
Measuring Range	0-200 ppm	0-1000 ppm	0-25% Vol	0-100% LEL 0-5% CH_4	0-100 ppm

The monitors have a limiting measurement range set for the sensors installed with values as shown in Table 4-3. The exposure limits are standardized OSHA regulations to reduce health risks in indoor air. Table 4-4 shows the maximum and minimum values that can be manually set for alarms.

Table 4-3 Standardized set alarm thresholds

Sensor	LOW alarm	HIGH alarm	STEL	TWA
COMB	10% LEL	20% LEL	--	--
CO	25 ppm	100 ppm	100 ppm	25 ppm
H_2S	10 ppm	15 ppm	15 ppm	10 ppm
O_2	19.5%	23%	--	--
NH_3	25 ppm	50 ppm	35 ppm	25 ppm

Table 4-4 Maximum and Minimum alarm set points for all sensors

Sensor	Minimum alarm set point	Maximum alarm set point	Default calibration values
COMB	5% LEL	60% LEL	58% LEL
CO	20 ppm	950ppm	60ppm
H_2S	5 ppm	175 ppm	20 ppm
O_2	5%	24%	15%
NH_3	15 ppm	75 ppm	25 ppm

4.2.2 Monitoring Toxic Gases

Toxic gases are monitored by the sensors; ammonia sensors were incorporated inside the instrument to display the gas concentration in parts per million (ppm) or mg/m^3. The instrument has four gas alarms.

- High Alarm
- Low Alarm
- STEL Alarm
- TWA Alarm

When the gas concentration reaches the alarm set point, the alarm message inside the instrument is displayed and the monitor flashes in combination with the resultant gas concentration. These alarms are set in accordance with OSHA (Occupational Safety and Health Administration)-PEL (Permissible exposure limits). The instrument also monitors the oxygen concentration from the gas sample, the alarm set points can be set to activate at enriched oxygen concentration >20.8% or deficient oxygen concentration <19.5%. Table 4-3 gives a list of maximum and minimum threshold values of alarm set points and the corresponding default calibration values of sensor. A number of environmental factors may affect the gas sensor readings, including changes in pressure, humidity and temperature. Pressure and humidity changes affect the amount of oxygen actually present in the atmosphere. An environment controlled chamber was utilized to avoid false alarms that occur due to changes in the barometric pressure or extreme changes in ambient temperature. Instrument operation is dialog driven from the display with the aid of three function buttons. A sampling safety test is available for instrument since it is equipped with an integral pump. Upon startup, a visual & audible alarm is triggered and the user is prompted to block the pumps/sampling system of the instrument within 30 seconds. When the instrument detects a pump flow block, it will display a ‘pass message’. The startup sequence will be resumed. If the instrument does not detect a pump flow block, it will display an error message. The instrument will shut off after the user acknowledges the message by pressing the up arrow button.

Instrument or sample line or probe shouldn’t be operated unless the pump alarm activates when the flow is blocked. In some cases sample may not be drawn to the sensors, which could cause lag in alarm indication, this should be avoided to minimize inaccurate readings. Never let

the end of the sampling line touch or go under any liquid surface. If liquid is drawn into the instrument, readings will be inaccurate and instrument could be damaged.

4.2.3 Calibration

Altair-5 multi gas detector calibration is done in order to maintain the consistency in results over time. Ammonia is a reactive toxic gas and the diffusion properties of the gas are active with materials such as rubber and plastic tubes. Leakages in the calibration gas before entering the sensors will not allow to duly perform instrument calibration, consequently certain prerequisites were taken before calibrating for ammonia,

- a specific pressure regulator inert to ammonia,
- short connection tubes between the pressure regulator and the instrument
- connecting tubes made from Poly Tetra Flouro Ethylene (PTFE) that doesn't absorb ammonia

Zero calibration is done by pressing the down arrow to confirm the zero screen, i.e. to execute zero calibration. Zero calibration begins; a progress bar shows the user how much of the calibration has been completed. After the zero calibration is completed the instrument displays Zero calibration pass. If the instrument passes the zero calibration the SPAN screen is displayed.

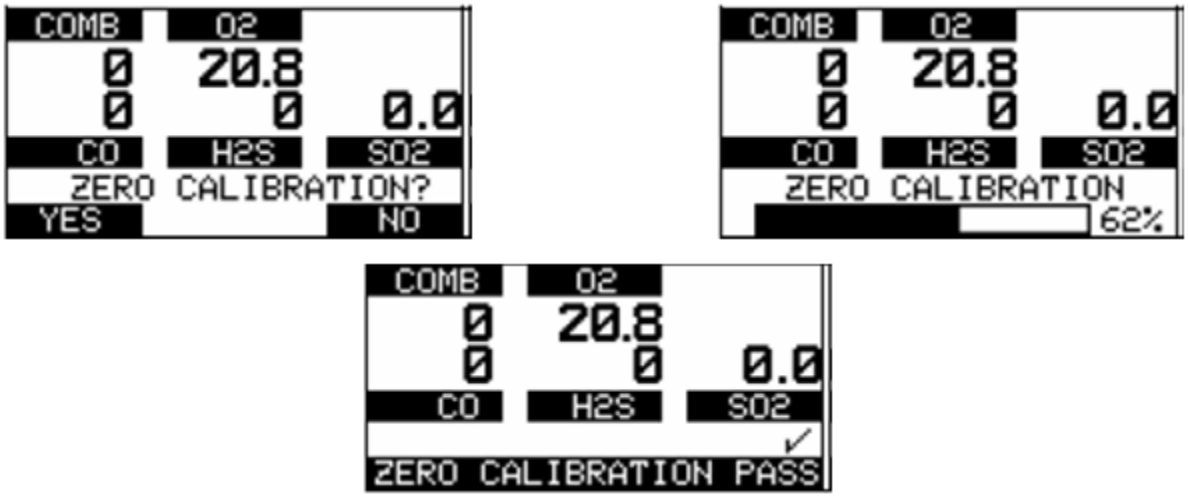

Figure 4-8 Altair-5 Monochrome display showing 3 steps in Zero calibration

Because of the different combinations of gases it is possible to perform single channel calibration for the exotic sensors such as NH_3. After the span screen is displayed, connect the standard 25 ppm ammonia calibration gas to the gas monitor. Attach the calibration cap to the gas monitor and open the valve on the regulator. The standard flow regulator is set to 0.25 liters

per minute. Press the down arrow button to calibrate the instrument. Span calibration starts blinking in the display; a progress bar shows how much of the calibration has been already been completed, after the span calibration is completed the instrument displays the message span calibration pass. Now close the valve on the regulator and remove the cap or tube from pump inlet. The calibration procedure adjusts the span value for any sensor that passes the calibration test. If the sensors fail calibration it is left unchanged. Since residual gas may be present, the instrument will briefly go into an exposure alarm after the calibration sequence is completed.

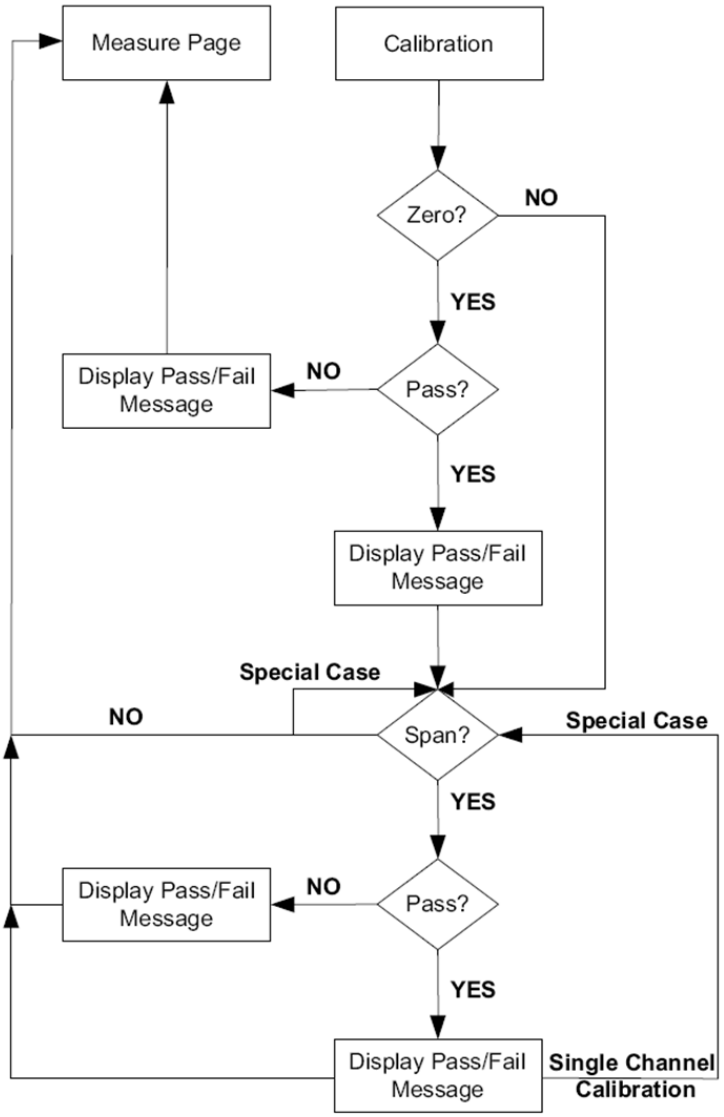

Figure 4-9 Flow chart for Calibration sequence

4.2.4 Differential Pressure Transducers

Pressure transducer PX653-05D5V (Omega Engineering Instruments) is used to monitor the pressure energy losses over the packed beds. This measure's the difference between two or more pressures introduced as inputs to the sensing unit. These measurements are utilized in obtaining correlation between pressure drop and flow rates. The accuracy of the pressure readings is ±0.50% (full scale) and the pressure range of this instrument is 0-5 inches of water. Operating temperatures are -20° to 160°F (-29° to 72°C) dependent on the type of strain gauge (capacitance) used in the transducer. The strain gauges are connected to form a Wheatstone bridge circuit to maximize the output of the sensor. These instruments have good repeatability of ±0.05% and response time is 250 ms. Specifications are listed below.

PX653 Voltage Output:

Excitation: 12-36Vdc

Output: 1-5Vdc

Supply Current: <5mA

Weight: 14oz. (397 g)

4.2.5 Volumetric flow rate meters

Flow meters used in this study are Dwyer model VFA-3 and RMB-51 ssv. These variable area flow rate meters are located at the inlet of the columns just after the pressure regulators in the gas/air flow line. Variable area meter consists of a tapered tube, with a black glass float inside that is pushed up by fluid flow and pulled down by gravity. As flow rate increases, greater viscous and pressure forces on the float cause it to rise until it becomes stationary at a location that is wide enough for the forces to balance. Float has been designed to spin visibly in the fluid stream to determine whether the float is stuck or not. The body is made of acrylic plastic for VFA-3 and polycarbonate for RMB-51-ssv. The accuracies are 5% and 3% full scale for VFA-3 and RMB-51-ssv respectively. The pressure and temperature limitations are however same for both the meters 100 psig (6.9 bar) @ 120°F (48°C).

During operation the valve is opened slowly to avoid possible damage. Control valves are turned clockwise to reduce flow, counter clockwise to increase flow. A nylon insert is provided in the threaded section of the valve stem to give a firm touch to the valve and to prevent change of setting due to vibration. The performance of low range units used in air or gas applications

may be affected by static electricity. Excessive static charge may cause the ball float to behave erratically or provide a false reading. To ensure the proper function of the unit, the application should be designed to minimize or dispel electricity.

The standard technique for reading a variable area flow meter is to locate the highest point of greatest diameter on the float, and then align that with the theoretical center of the scale graduation. In the event that the float is not aligned with a grad, the operator as to its location between the two closest grads must make an extrapolation of the float location.

4.2.6 Pressure Regulator

Pressure regulator is installed to control excessive pressures and reduce noise in the system. Control air inc., 0-10 psig ranged regulator is assembled in the facility. Rotating the adjusting screw changes the force exerted by the spring on the diaphragm assembly inside the regulator. In equilibrium of set pressure, the force exerted by spring is balanced by the force from the output pressure acting below the diaphragm. An unbalanced state between the output pressure and the set pressure causes a corresponding reaction in the diaphragm. If the output pressure rises above the set pressure, an upward force is exerted on the diaphragm causing the relief seat to lift and open. Excess pressure is vented to atmosphere until equilibrium is reached. Similarly if the output pressure drops below the set pressure the unbalanced force of the spring causes a downward force on the diaphragm. The supply valve then opens until the pressure builds up once more to the equilibrium condition. Under forward flow conditions, the spring force is balanced by the diaphragm pressure force, with the supply valve open just enough to maintain the required equilibrium pressure. Maximum supply pressure limit that can be handled is 250 psig (1700 kPa). The regulator is mounted on the wooden frame and connected to the pipe from the compressor and passes the flow into the facility. The exhaust capacity is 0.1 scfm with downstream pressure 5 psig above set point

4.2.7 Data Acquisition

Data acquisition unit HP 34970A was used to convert the transducer readings in voltage. The digital multi-meter inside the unit can measure voltage, current, resistance and temperature. Once the calibration was performed, the slope and intercept of the calibrated data were programmed inside the data acquisition unit and thus the data was normalized.

The IFSYS-8004 USB Serial-IR Adapter is used for transfer of raw serial data wirelessly over a serial infrared link. IFSYS-8004 comes with a USB driver that appears as a virtual serial port in the host system, allowing existing serial applications to work with little or no modification. IFSYS-8004 hardware simply encodes the serial data stream into IrDATM physical layer infrared pulses for transmission and demodulates incoming infrared pulses into serial UART (universal asynchronous receiver/transmitter) data. UART's are commonly used in conjunction with communication standards such as RS-232, RS-422 and RS-485. Data between host and adapter is transferred over the USB link. The adapter works with raw serial data and supports SIR (serial infra red) communications speeds up to 115,200 bps. The communication through desktop is done using MSA Link-v1.0.5.0 software.

Dimensions:

Casing: 49mm (W) x 63mm (L) x 34mm (H)

Cable length: 1.5m

Weight: ~120g

4.3 Experimental Methodology

The compressed air supplied from the compressor flows through the hose and enters the column at an inlet diameter 0.75 inches. And the resultant pressure drop measurements were taken over the length of the packed bed. The differential pressure transducer measures the pressure at two points, one at the inlet and the other at the exit of the bed. Wire mesh sieves were used at both the ends of the bed in order to avoid loss of material. In addition the wire mesh provides uniform packing at the inlet and outlet of the column and helps minimize random errors during experiments.

4.3.1 Procedure for packed bed column1

- Flow rate of compressed air is recorded with a commercial flow rate meter that converts the measurements in SCFH (Standard Cubic Feet per Hour). Volumetric flow rates were varied over a range of 2 to 12 SCFH
- Pellet materials are arranged in the packed bed architecture for pressure flow characterization.

- Pressure taps are placed upon the packed bed which increased the accuracy of the reading by reducing the noise caused due to sudden expansion/contraction of air.
- Pressure drop across the bed is measured with a differential pressure transducer and digitally monitored using data acquisition/switch unit (Hewlett Packard 34970A).

4.3.2 Nitrogen Sorption test

- The sample is degassed using highly pressurized control environment for 1+ hours.
- Weight of the degassed sample is measured using weigh balance and the mass readings were noted.
- The sample is kept in a test tube bulb at 77K using nitrogen bath. The tube is fixed in the BET tester and is connected to nitrogen supply line using adjustable screw and o-rings.
- The inert vapor is sent into test tube and the amount adsorbed over time is calculated at different partial pressures of influent gas.
- To the resulting adsorption isotherm, BET theory is applied(by simulation software) to calculate the specific surface area
- From this information using BJH theory the pore size distribution is obtained and the dominant pore size in the material was around 3 nm.

4.3.3 Procedure for Packed bed column2

- Open the tapered glass fitting at the inlet of the column tube and load the Nanoparticles slowly on the silica matrix.
- Adsorbent material is loaded for a given packing height and the column is joined by closing the screw fit assembly provided. O-ring should be adjusted to prevent leakages from the column
- Ammonia gas tank (Matheson tri-gas) is connected to a high purity single stage pressure regulator (Linweld Corporation) and the regulator pressure is decreased to zero inches of mercury at the inlet.

- The valve on the cylinder is fully opened and the pressure regulator is rotated to slowly increase the pressure and thereby creating a controlled steady flow. A known concentration of ammonia (50 ppm) is delivered to the bed at a known delivery rate.
- Gas flow was established and passed through volumetric flow rate meter (Dwyer instruments) and the flow rate was set to the desired value at room temperature (23±1 °C)
- Steady flow velocities were set within the range of 0.5 SFCH and 5 SCFH; these values are representative of flow rates utilized in aircraft cabins.
- Adsorbate gas is passed down from column top to bottom, here an interaction between adsorbent-adsorbate takes place. The adsorbent column is a glass cylinder , 19mm in diameter and 17mm in height
- The inlet concentration was set to 50 ppm in all cases, since there is no indicated influence of inlet concentration on rate constant.
- Filtered flasks were installed into the gas flow pipe line just before the flow meter and at the exit of the column to sample gas concentrations over time
- Inlet and outlet concentrations of ammonia were sampled using Altair-5 multi gas detectors and a real time continuous data was generated until equilibrium is achieved between the two phases. These instruments provide with an instantaneous concentration of adsorbate (which is preferred for effluent concentration readings).
- The data is collected inside the Altair-5 gas monitors and saved in the memory card. IFSYS-8004 USB Serial Infrared adapter is used for data retrieval from gas monitor to personal computer through MSA link software.
- Varying packing heights were tested using the facility-2 and the time to adsorbate breakthrough and the amount of adsorbent in the bed were recorded.
- If the adsorbate starts to penetrate immediately, the experiment must be stopped and more material ought to be added since the bed height is not equal to critical bed depth (which is normally the case), or change the experimental conditions.

Chapter 5 - Results and Discussion

This chapter presents the experimental results obtained during different phases of the research study. Pressure drop measurements through packed beds for varying flow rates are obtained for the estimation of energy losses. Pressure drop for flow through packed beds is presented in Section 5.1. Section 5.2 deals with the surface area characterization of adsorbents. Breakthrough curves are presented in Section 5.3. The organization of the section includes data collection using chemical sensing techniques, breakthrough curves for the variation of flow-rates and length of the column and the calculation of adsorption rate parameters.

5.1 Pressure drop for flow through packed beds

Fluid flow through two different types of packed bed columns are studied in these experiments. Experimental data for two types of packing materials (Activated Carbon and Zirconium marbles) with different shapes (cylindrical and spherical) and varying packing heights were compared to Ergun equation and Idlechik predictions. Measurements for pressure drop were performed for varying flow rates.

5.1.1 Pressure drop versus flow rate measurements for cylindrical shaped carbon pellets

The dependence of pressure drop on flow rate as a function of porosity is identified in the foregoing results. Figure 5.1 shows the correlation between pressure drop and volumetric flow rates for distinct amounts of carbon pellets. Readings were taken for the change in flow rates within the range of 0 to 15 SCFH. Four different bed lengths (20mm, 57mm, 92mm, and 140mm) are evaluated in the fixed bed. The data were monitored by the data acquisition unit coupled with the differential pressure transducers. Recorded data show an exponential correlation with good approximation (R^2= 0.97±2). Experiments were also done with empty columns and the data were normalized accordingly (Appendix).

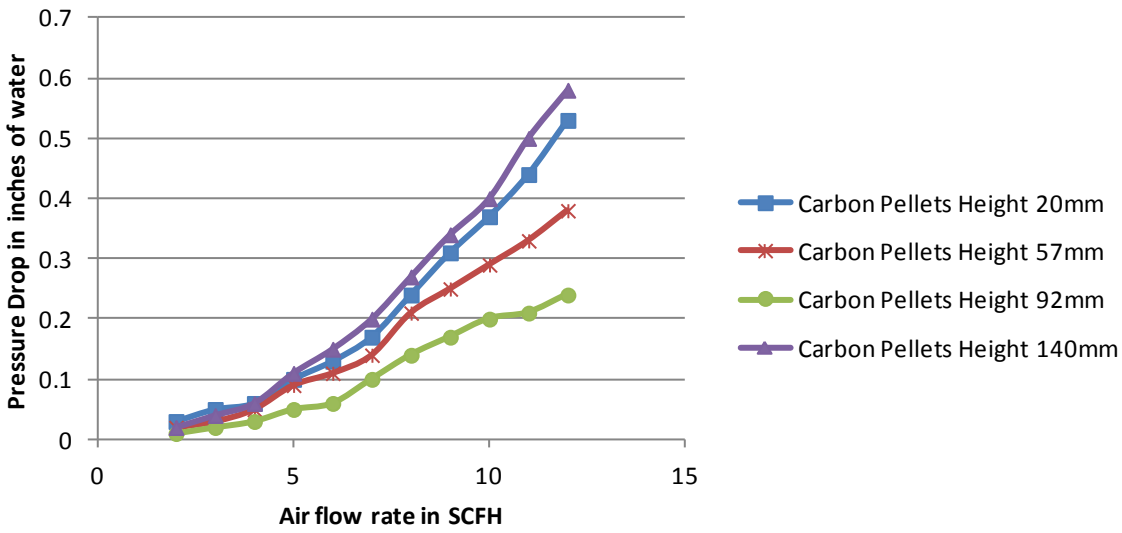

Figure 5-1 Correlation between pressure drop and volumetric flow rates

The packed bed is randomly packed with cylindrical pellets, the void fraction of the column is determined as the space in between the pellets after packing. Though the activated carbon is porous in nature, the intra-pellet porosity is not taken into consideration for the calculation of volume fraction as the relative effect of micro pores is negligible on the overall effect of pressure drop. Variation between pressure drop and flow rate follows a generalized exponential trend for each packing height. This trend is logical as the packed bed consists of porous media [22].

5.1.2 Micro-scale balance measurements for cylindrical shaped carbon pellets

Micro-scale balance was used to measure the mass of 9 random samples of Activated Carbon. Sartorius micro scale measurements are shown in the Table 5-1. The height of each pellet was measured using a digital vernier caliper and measurement was taken for an average of three readings. Average density of the material was approximately 0.984 mg/mm^3. This density of material is the bulk density which includes the particle volume, inter-particle void volume and internal pore volume. Calculation of the bed porosity was done considering the material as bulk quantity and the values are in the range of 0.5±0.07.

Table 5-1 Microbalance measurement for each cylindrical pellet

Sample	Activated Carbon unit mass (mg)	Height (mm)	Radius(mm)	Volume of each cylinder(mm^3)	Density (mg/mm^3)
1	125.5	9.64	1.90	109.32	1.14
2	131.74	13.73	1.99	170.81	0.77
3	119.50	7.49	1.88	81.16	1.43
4	92.50	9.64	1.90	109.32	0.84
5	81.00	7.09	1.87	78.30	1.03
6	99.30	9.86	1.85	106.01	0.93
7	78.20	7.30	1.93	85.86	0.91
8	82.10	8.42	1.91	97.00	0.84
9	61.00	5.77	1.90	65.78	0.92
Average	96.76	8.77	1.90	100.39	0.98

5.1.3 Pressure drop variation as a function of volume fraction

In this section pressure drop variation as a function of volume fraction is examined. Volume fraction (VF) is the portion of material present in the total volume available, i.e., solid concentration.

$$\boldsymbol{VF = \frac{Vsolid}{Vsolid + Vvoid}} \tag{5.1}$$

Pressure drop measurements were taken for 11 different flow rates 2, 3, 4, 5, 6, 7, 8, 9, 10, 11, 12 SCFH. There is a steady increase in pressure loss profile with increase in flow rate. The dependence of pressure drop and flow rate remained the same without any trends as for the variation in volume fractions. The correlations between pressure drop and flow rates maintained an exponential function.

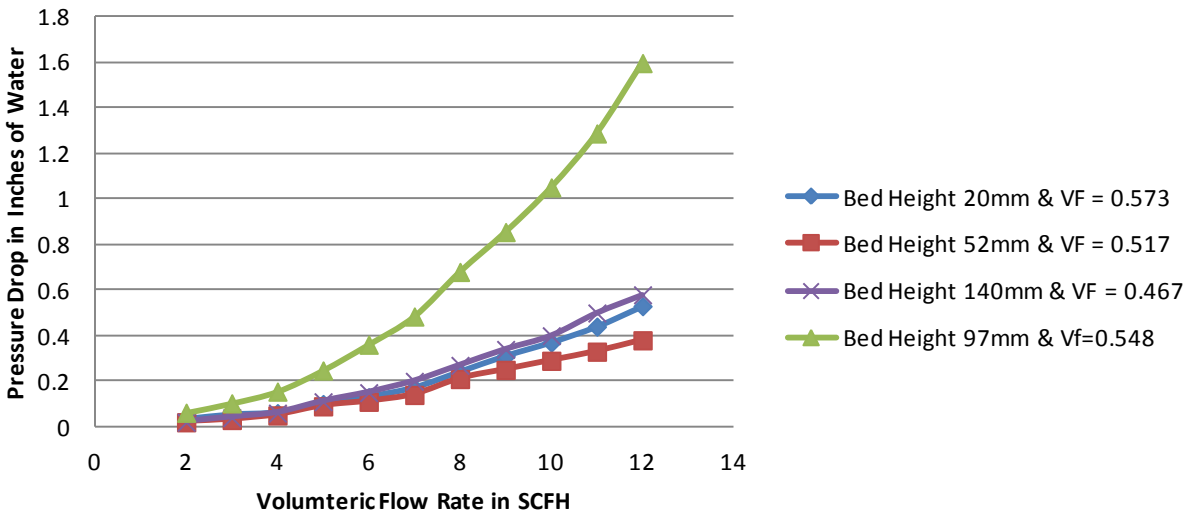

Figure 5-2 Correlation of pressure drop and volumetric flow rate as the function of material concentration by volume fraction

5.1.4 Pressure drop over length as a function of volume fraction

From the discussion in Section 5.1.1, it is apparent that the correlation between pressure drop and volumetric flow rate did not show the effect of volume fraction. This time experimental curves were drawn again by replacing the ordinate to Pressure drop over length; this includes the effect of length on the pressure drop for variable porosities. Flow measurements were taken in SCFH at the inlet of the fixed bed column and their corresponding values of pressure drop by length labeled as $(\Delta P)/L$ in (inches of H_2O)/inches. The significance of the correction of y-axis parameters can be observed in Figure 5-3. The corrected values are shown in Table 5-2.

Table 5-2 Correction parameters for flow through packed bed

Flow Rate in SCFH	ΔP1/L1	ΔP2/L2	ΔP3/L3	ΔP4/L4
12	2.65	0.73	1.59	0.41
11	2.20	0.63	1.28	0.35
10	1.85	0.55	1.05	0.28
9	1.55	0.48	0.85	0.24
8	1.20	0.40	0.68	0.19
7	0.85	0.26	0.48	0.14
6	0.65	0.21	0.36	0.10
5	0.50	0.17	0.24	0.07
4	0.30	0.09	0.15	0.04
3	0.25	0.05	0.10	0.02
2	0.15	0.03	0.06	0.01

There is a systematic orderly placement of curves relative to their volume fractions as shown in Figure 5-3. These curves tend to towards the y-axis with an increase in volume fraction. Packed bed with volume fraction 0.573 shows a higher value for the pressure drop at a given flow rate compared to other beds with volume fractions 0.548, 0.517 and 0.467. These results are significant theoretically and will be discussed further.

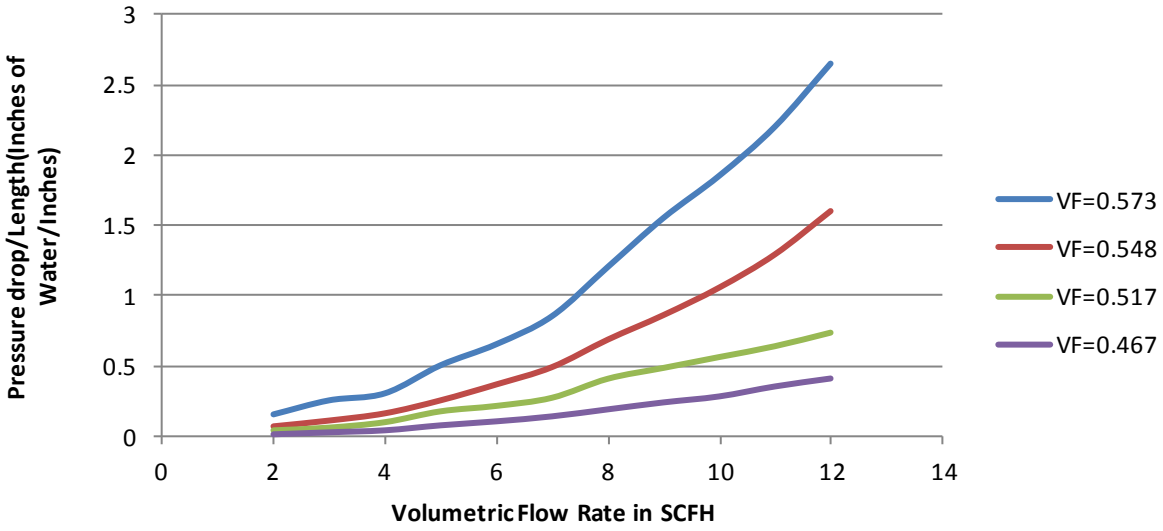

Figure 5-3 Correlation of pressure drop over length and volumetric flow rate as a function of volume fraction

5.1.5 Reynolds Number and friction factor

The pressure drop and flow rate measurements were transformed into friction factor and Reynolds number to compare with Ergun's equation (Figure 5-4). Effect of viscosity of air over temperature was considered and Sutherland's conversion was employed for the identification of Reynolds number at 25°C (Appendix A.2.2).

The friction factor was calculated using the equation [24]

$$F_p = \frac{\Delta P}{L}\frac{D_p}{\rho V_s^{\,2}}\left(\frac{\varepsilon^3}{1-\varepsilon}\right) \tag{5.2}$$

This requires the Reynolds number to be between 10 and 1000.

Ergun equation is a superimposed version of Blake-Kozeny equation and Burke-Plummer equation for laminar and turbulent flows respectively. Ergun tested for different materials and varying flow rates and obtained the equation in simplified parameters of friction factor and Reynolds number as follows [24]

$$f_f = \frac{150}{Re_p} + 1.75 \tag{5.3}$$

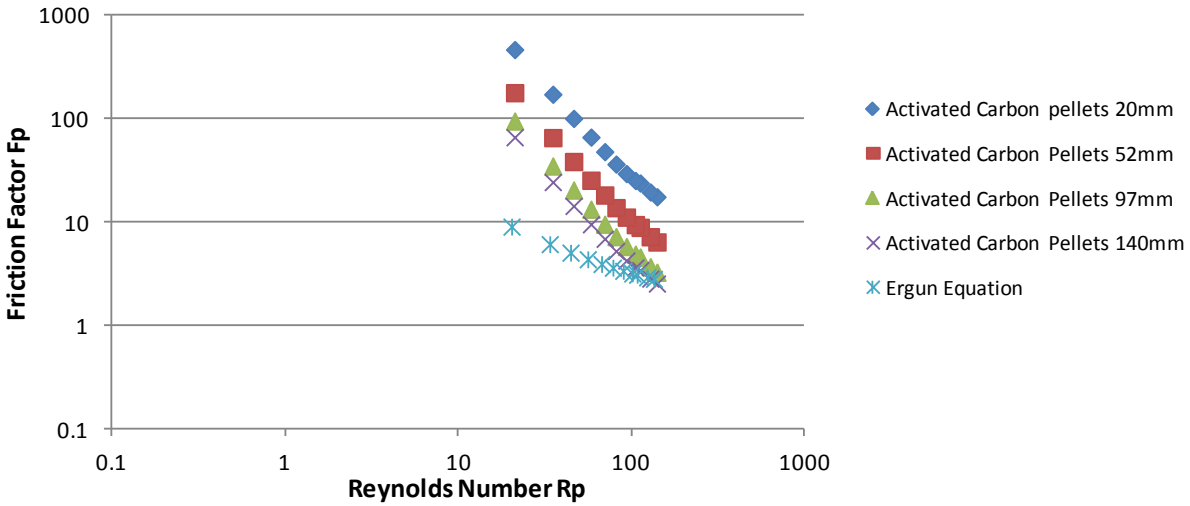

Figure 5-4 Friction factor Versus Reynolds Number

Ergun's data was compared with the above results with a good approximation. Ergun equation is more accurate for rough surfaces such as gravels and pellets. As the curve approaches lower Reynolds number (100 to 10) there is a deviation in the curves. One source of deviation is the porosity of the packed bed; the above experiments did not take into account the internal porosity of activated carbon to be significant enough since the subject gas is nitrogen. Nitrogen gas is chemically inert and we assumed there is no stagnation of the molecules inside the pores which is an ideal case. The other source of error is the effect of temperature on the viscosity of gas. Though Sutherland's conversion was employed to minimize the effect of viscosity there will be fluctuations in the room temperature that adds to the error in measurements.

5.1.6 Pressure drop versus flow rate measurements for spherical zirconium marbles

Variation of pressure drop with flow rate is observed to be quadratic in nature. Vacant column was tested for pressure drop in the channel and the results are compared with packed bed results. Ergun's equation is a good approximation for rough surfaces like pellets and gravel etc., for smooth surfaces such as zirconium marbles Idlechick method is preferred. The data was compared with Idlechik predictions [26] as shown in Figure 5-5. Pressure taps were placed on the packed bed to reduce the noise caused due to sudden expansion and contraction of air flow.

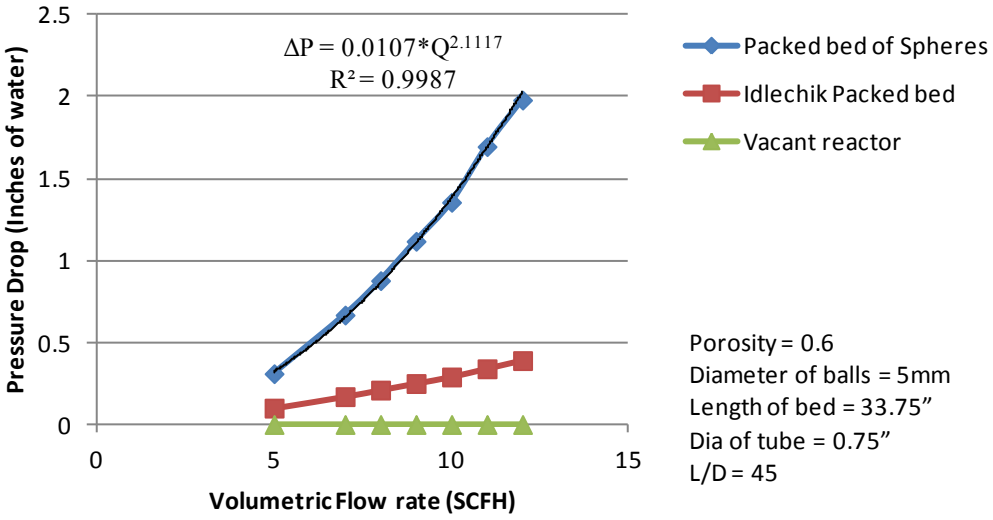

Figure 5-5 Pressure drop versus flow rate for spherical zirconium balls

5.1.7 Idlechik Predictions and data comparison

Pressure drop is a strong function of diameter of the balls composed in the bed. For 7 different diameters of spheres theoretical pressure drop is measured on the basis of *Idlechik* predictions as shown in Table 5-3.

Table 5-3 Measurement of pressure drop variations as a function of sphere diameter

Diameter of Zirconium spheres	ΔP1	ΔP2	ΔP3	ΔP4	ΔP5
5	0.10	0.16	0.24	0.39	0.65
4.5	0.12	0.19	0.29	0.47	0.78
4	0.15	0.23	0.35	0.57	0.95
3.5	0.19	0.29	0.44	0.71	1.19
3	0.24	0.37	0.58	0.93	1.55
2.5	0.33	0.51	0.79	1.27	2.13
2	0.49	0.75	1.17	1.89	3.17

The curves showed a decreasing response in pressure drop from least diameter to highest diameter spheres. Porosities for each packed bed is calculated from equation

$$n = 1 - \frac{\pi}{6.(1-\cos\theta).\sqrt{(1+2\cos\theta)}} \tag{5.4}$$

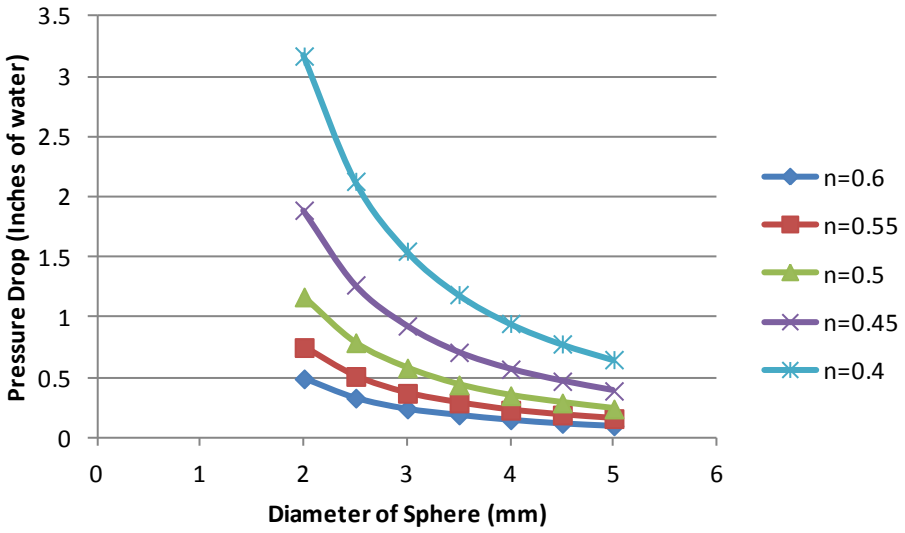

Figure 5-6 Pressure drop as a function of diameter of spheres

5.2 Nanoparticle Characterization

5.2.1 BET (Brunauer, Emmett and Teller) test for surface area measurements

Adsorbent samples were degassed at 100° C with a vacuum pump prior to BET measurements. Nitrogen isotherms for the samples of 0.05(± 0.01) gm were analyzed within nitrogen bath at a constant temperature of 77 K. Liquid nitrogen was poured in a thermo-flask and vapors released maintained the outside temperature of the bulb. The surface area, BET microporous volume, mesoporous volume and total pore volume were calculated from the isotherms. Pore size distribution was obtained from the adsorption-desorption analysis. These tests indicated the physical characteristics of novel materials under study from the same testing device to minimize calculation errors. BET test is generally employed for calculating surface area of materials. This theory assumes that gas molecules stick to the solid surface in more than one layer and further there is no interaction between layers of adsorption.

BET equation

$$\frac{\mathbf{1}}{\boldsymbol{\nu}\left\{\left(\frac{\boldsymbol{P}}{\boldsymbol{P_o}}\right)-\mathbf{1}\right\}}=\frac{\boldsymbol{c}-\mathbf{1}}{\boldsymbol{\nu_m c}}\left(\frac{\boldsymbol{P}}{\boldsymbol{P_o}}\right)+\frac{\mathbf{1}}{\boldsymbol{\nu_m c}} \tag{5.5}$$

where P and Po are the equilibrium and saturation pressures of the adsorbates at the temperature of adsorption, ν is the adsorbed gas quantity, and ν_m is the monolayer adsorbed gas quantity. c is the BET constant

$$\boldsymbol{c}=\boldsymbol{exp}\left(\frac{\boldsymbol{E_1}-\boldsymbol{E_L}}{\boldsymbol{RT}}\right) \tag{5.6}$$

where E_1 is the heat of adsorption of the first layer, and E_L is counterpart for the second and multi-layers above and is equal to the heat of liquefaction. As nitrogen adsorption isotherms were used to characterize the surface area and micropore volume. This data used the standard method applied over the relative pressure range of 0.01-20 inches of water. The micropore volume was calculated by applying the Dubinin-Radushkevich equation [23] to the isotherm.

Table 5-4 Physical properties of Adsorbents from Nitrogen Adsorption

Adsorbent	Surface Area(m^2/g)	Pore Volume(cm^3/g)
Norit RZN01	$4.6x10^2$	$8.81x10^{-2}$
Norit Vapure 410	$9.01x10^2$	$2.36x10^{-1}$
Norit RB40M	$8.10x10^2$	0.196
NanoActive™ MgO	$2.42x10^2$	$3.24x10^{-1}$
NanoActive™-G MgO	n/a	n/a

The results obtained from the determination of surface area and pore volume of Norit based carbonaceous compounds and NanoActive™ materials are presented in Table 5-4. From this, it can be seen that Norit compounds have high surface areas ($4.6x10$ m^2/g ^{2},$9x10^2$ m^2/g, $8.1x10^2$ m^2/g) compared to NanoActive™ MgO and this is usually the reason for carbon compounds to be selected for many industrial adsorption applications. The meso pore volume obtained for NanoActive™ materials is almost 3 times the pore volume of RZN 01. It would be interesting to study if a Metal Organic Framework (MOF) is established for NanoActive™ materials that can inhibit strong structural properties to compete with graphene materials in surface structural properties.

5.3 Breakthrough curve results

These results show the successive dynamic breakthrough curves obtained by the real time monitoring of the fixed bed column experiments. This method gives the instantaneous concentration of adsorbate in the effluent (relative to the inlet concentration). The test conditions are standardized to be more relative to the application of IAQ enhancement chambers that use very low flow-rate inputs for the purpose of this research study. Time at which an adsorbate of defined concentration is able to penetrate the bed is known as breakthrough time. The key factor in this is the service life of the filter, which is defined as the time at which the concentration of the compound penetrating the filter reaches an unacceptable level. An accurate estimation of service life is of great importance. S.I units were used for convenience of calculations from section 5.3.1.3. Conversion factors are discussed in Appendix A.2.1.

5.3.1 Flow-Variable BTC's

This section presents the experimental data for unique set of materials selected for this study; breakthrough curves of ammonia for an inlet concentration of 50 ppm subjected to activated carbon for variable flow rates is shown in Figure 5-7. The packed bed material was tested for volumetric flow rates of 0.497 L/min, 0.94 L/min and 1.41 L/min. A breakthrough was observed for the lowest flow rate of ammonia and with an increasing trend in flow rates there was not enough contact time for proper adsorbate-adsorbent interaction. Within 37 minutes breakthrough was observed for a flow rate of 0.497 L/min and the length of the bed is 2 inches (~ 50 mm). There is an earlier breakpoint and tailing in breakthrough curves with increase in flow rates. The breakthrough curve reaches equilibrium at 0.7 Co/Ci and not at 1 Co/Ci; the reason might be that the moisture content inside the adsorbent is higher than that of the moisture of the adsorbate.

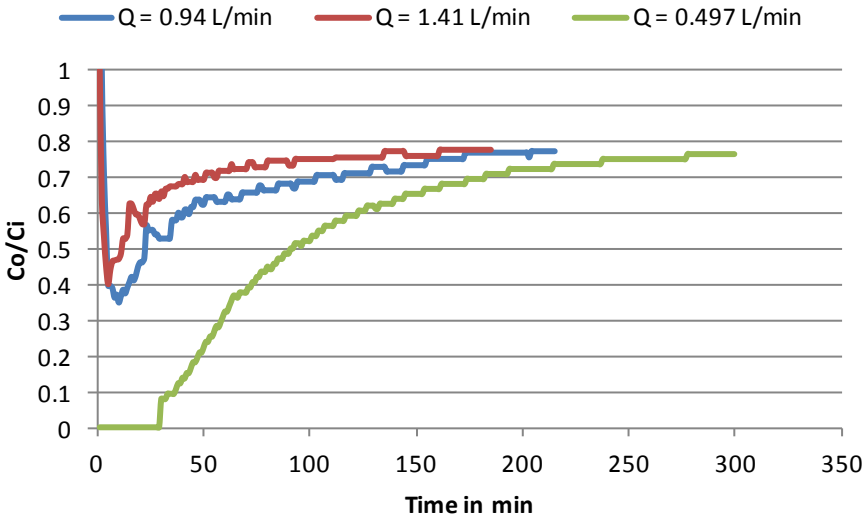

Figure 5-7 Breakthrough curves of ammonia against activated carbon

Equilibrium is said to be attained when adsorbent is completely saturated with the adsorbate molecules. The test facility used for the characterization of nanomaterials was tested with an empty column to estimate the equilibrium curve for the experiments. From the Figure 5-13 it is estimated that when the breakthrough curve reaches around 0.8 of Co/Ci fraction, saturation of adsorbent is complete. The repeatability of the facility is shown in Figure 5-8 with activated carbon as adsorbent at 0.497 L/min for 2 runs and they represent almost the same

curves within 5% percentage error. This shows a good response of the complete facility for the repetition of experiments.

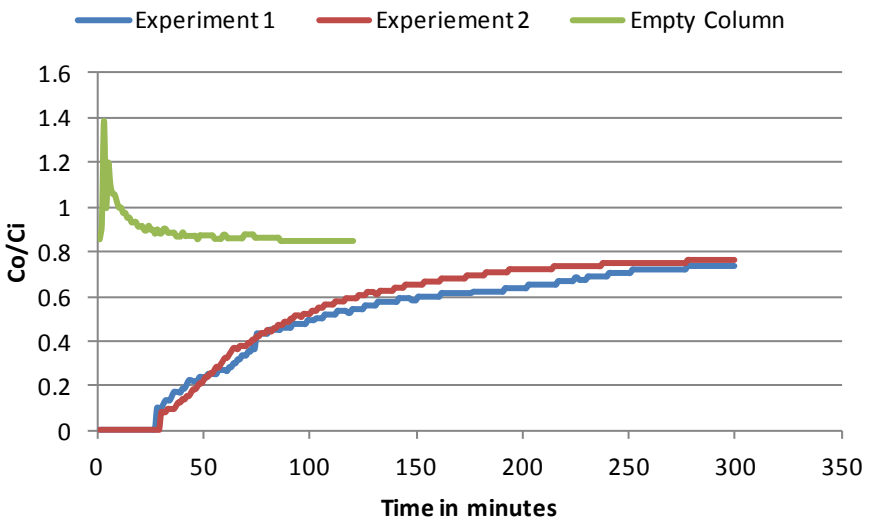

Figure 5-8 Repeatability and empty column experiments

Breakthrough curves for activated carbon show a spike starting from Co/Ci fraction of 1 in Figure 5-8. These curves usually occur due to noise in the instrument. The gas sensing device measuring the outlet concentration started to read a higher concentration than that of the inlet concentration. Sometimes accumulation of ammonia gas inside the filtered flasks can cause such disturbances in the initial stages of breakthrough curves. To avoid the occurrences of this sort of data, filtered flasks were cleaned and the left over ammonia gas from previous runs was discharged by exposing the flasks to atmospheric air. The inlet concentration profile and outlet concentration profile of the curves obtained from Figure 5-8 for a flow rate of 0.94 L/min is shown in Figure 5-9. Figure5-9 clearly shows that a small initial jump in outlet concentration caused the noise seen in Figure 5-8. Figure 5-10 shows data for 0.497 L/min. This data is more typical with outlet concentration staying at 0 for approximately 30 minutes.

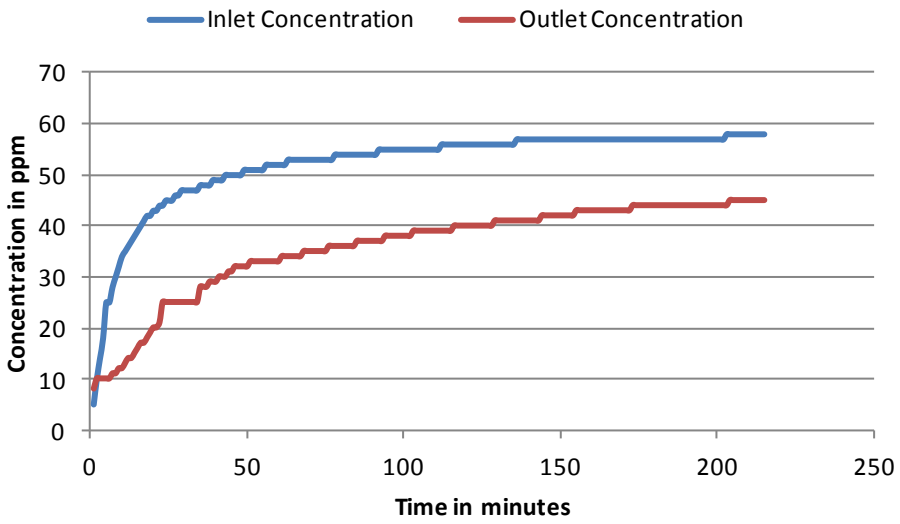

Figure 5-9 Inlet and outlet concentration profiles for activated carbon breakthrough curve at 0.97 L/min

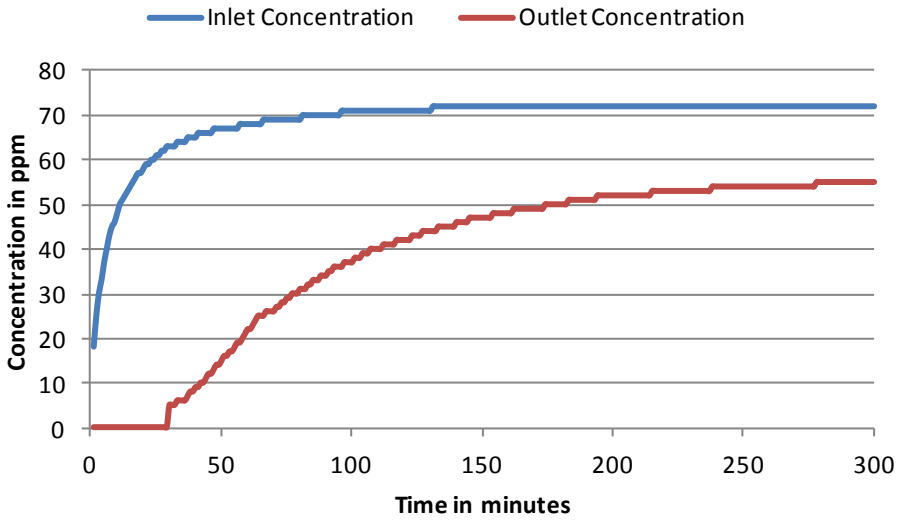

Figure 5-10 Inlet and outlet concentration profiles for activated carbon breakthrough curve at 0.497 L/min

For activated carbon at flow rate of 0.497 L/min (Figure 5-10) there was no significant noise observed after taking the precautions mentioned above. This signifies that the range of flow rates that can be utilized in the facility varies for a given material and is relative to its shape, porosity and structural properties.

5.3.2 Norit RZN01

Norit RZN01 was tested for three different flow rates 0.51, 0.98 and 1.53 L/min for a bed length of 50 mm. Breakthrough times were achieved ahead of time compared to other materials. For the amount of material in the bed RZN01 shows a near steady state or equilibrium reached between two phases at 30% of the outlet to inlet concentration ratio. The corresponding breakthrough times for the runs in increasing order for flow rates are as follows 77, 52, 29 minutes. Increase in flow rates decreased the breakthrough times in all variable flow rate test runs.

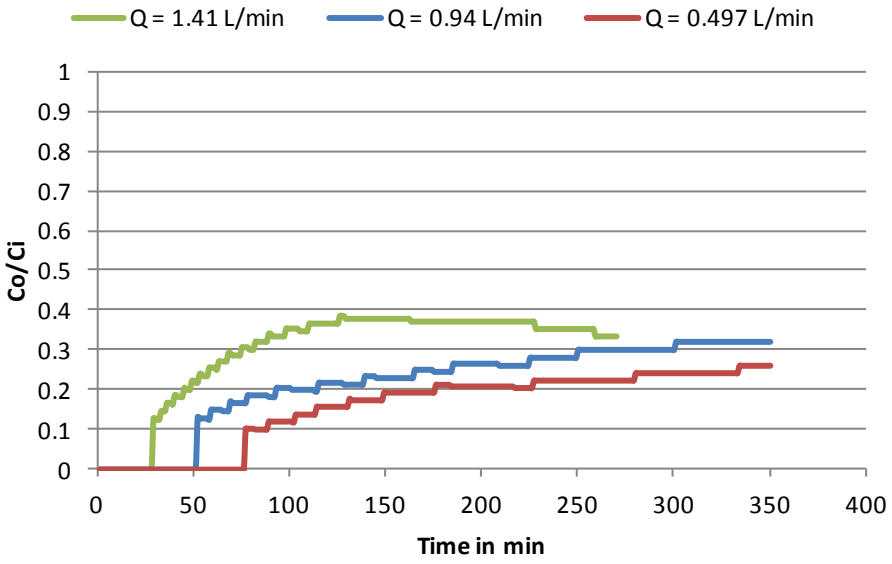

Figure 5-11 Breakthrough Curve of Ammonia against Norit RZN01 for variable flow rates

Residence time of the bed and time to 1% breakthrough time were plotted to test for linearity of adsorption capacity over variation of flow rates as show in Figure 5-12. The plots drawn indicate the variation for the given percentage of breakthrough. Early breakthrough percentages are most convenient in exploring the adsorption kinetics, since it shows the immediate effect of the phase interactions where the saturation capacity of adsorbent starts to deplete.

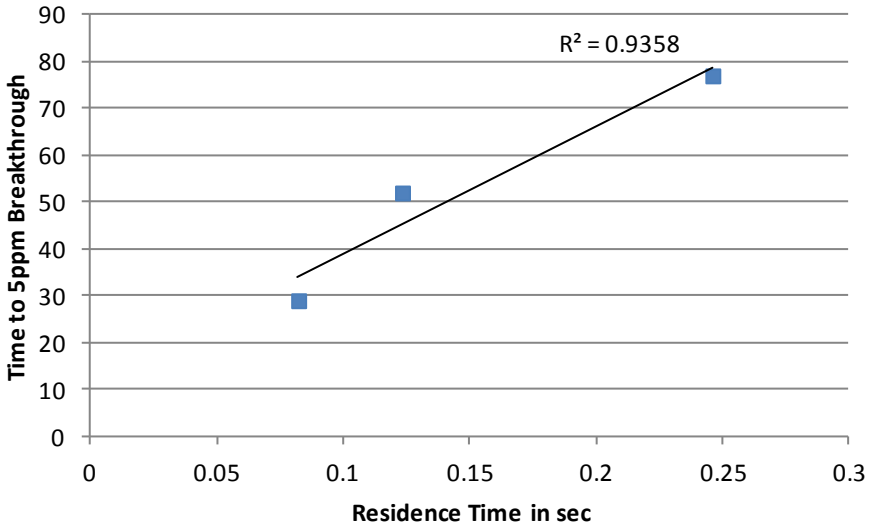

Figure 5-12 Time to breakthrough versus Bed Residence Time for Norit RZN01

Residence time (in seconds) is the bed depth divided by the superficial velocity which can be expressed in terms of volume of the bed V in cm^3 and the flow rate Q in L/min as follows

$$\boldsymbol{\tau(s) = 0.06\left(\frac{V}{Q}\right)} \qquad (5.7)$$

Since the relation between time to percentage breakthrough and residence time is linear this implies a dynamic adsorption capacity almost independent of the flow rate under the conditions of the test runs.

5.3.3 NanoActive MgO

NanoActive MgO was packed in the specialty test facility to test for variable flow rates. The length of the bed was kept at 0.5 inch to prevent high pressure drops due to the density of powder packing. Flow rates were varied for four different runs and the values are 0.8,1, 1.4 and 2 SCFH. There was a gradual shift of breakthrough time towards origin with increase in flow rates as more ammonia is fed over the same time and the saturation limits are reached earlier. Breakthrough times observed for each flow rate of 0.8, 1, 1.4 and 2 SCFH are 74, 60, 22, and 18 in minutes respectively.

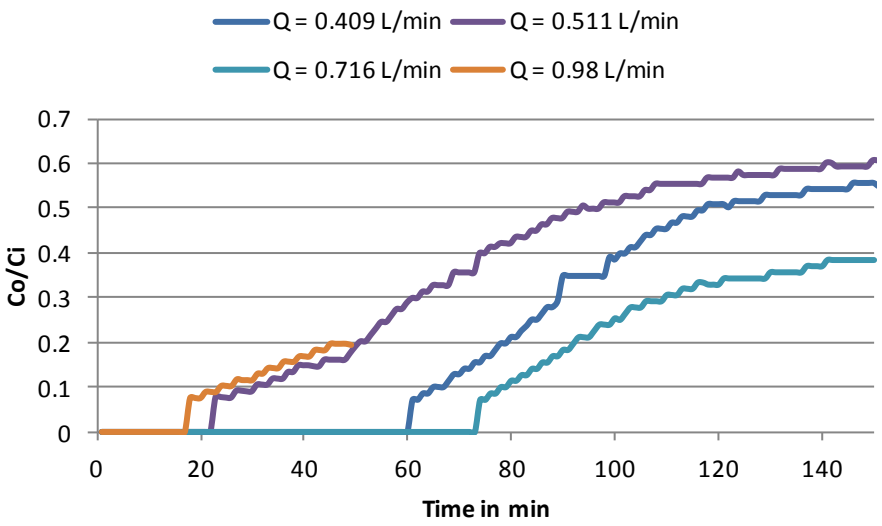

Figure 5-13 Breakthrough curves of NanoActive^{TM} MgO for variable flow rates

The test run with 0.409 L/min was stopped before it could reach equilibrium due to the fact that the amount of pressure induced into the test facility crossed over its limit. There was a back flow into the inlet filter flask which was observed around 45 min and the test was halted. This provided us with an insight as to accelerate the test without disrupting the structural morphology of the nanomaterials.

The desired application requires maintenance of ammonia concentration to be around 50ppm. Efforts were made to keep all the variables near constant except the flow rates, though this will affect the adsorption kinetics and consequently the adsorption rate, the adsorption capacity will not change as it is the property of adsorbent-adsorbate interaction. From the results obtained from Figure 5-14, data is plotted as time to breakthrough time versus residence time. The range of flow rates that were measured was from 0.409L/min to 0.98 L/min for NanoActive MgO for a bed length of 12.5 mm.

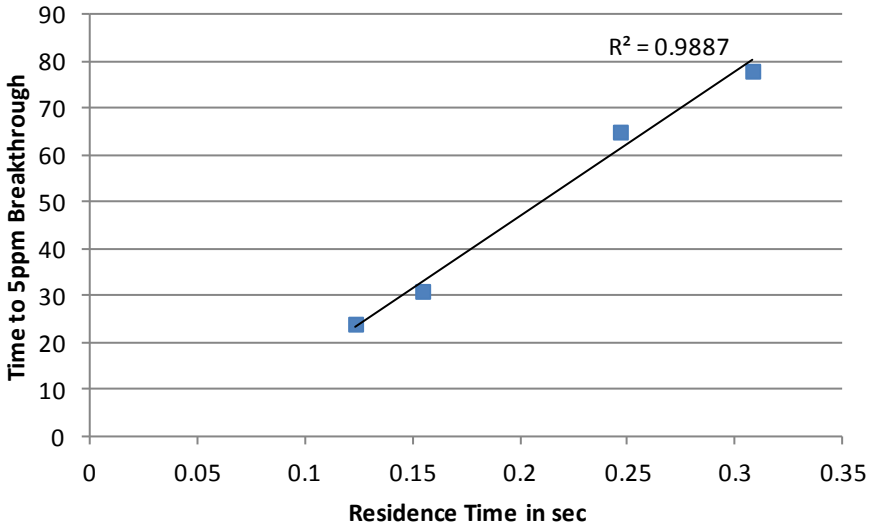

Figure 5-14 Time to Breakthrough versus Residence time for NanoActive MgO

5.4 Mass-Variable BTC's

These tests represent the variation of amount of material in the packed bed columns subjected to 50ppm of ammonia gas. Column experiments were performed using a 50ppm concentration of ammonia gas (Linweld Corp.) supply with balance air. Five materials with known properties are tested for saturation limits and in turn to estimate their service life in filtration of Ammonia.

Norit RZN01, Norit Vapure 410, NanoActive MgO and NanoActive MgO-Granular (G) and Nanozorb are tested for breakthrough times with length of the bed as variable for constant flow rates. Ammonia gas was process fed through the test facility and a mixer for reliable monitoring of the concentration. Filtered glass flask of 1000ml was used to mix the gas well before monitoring, and the inlet of catalytic monitoring device was integrated into one of the outlets of the flask.

5.4.1 Norit RZN01

Four varied bed lengths of 5, 10, 15, and 30 mm were tested for adsorption kinetics for a constant flow rate. Ammonia gas with balance air at 50 ppm was supplied continuously with downward flow in the column at a flow rate of 1.53 L/min. The flow rate was adjusted by a specialty pressure regulator for the ammonia and was maintained at the desired value. The

effluent was measured periodically over time using a multi-gas detector (MSA) coupled with ammonia sensors. This material was specifically manufactured for the application of Ammonia gas removal and the breakthrough times were 29, 83, 196 and 311 minutes respectively with increasing height of packed bed. Since the mass transfer zone increases with increase in the length of the bed, saturation of the material and penetration of ammonia is delayed over time and a greater breakthrough time is achieved for each experiment as shown in Figure 5-15.There is a steady state like behavior after breakthrough's were achieved, though the material is not saturated completely which can be attributed to the doping for gas extraction.

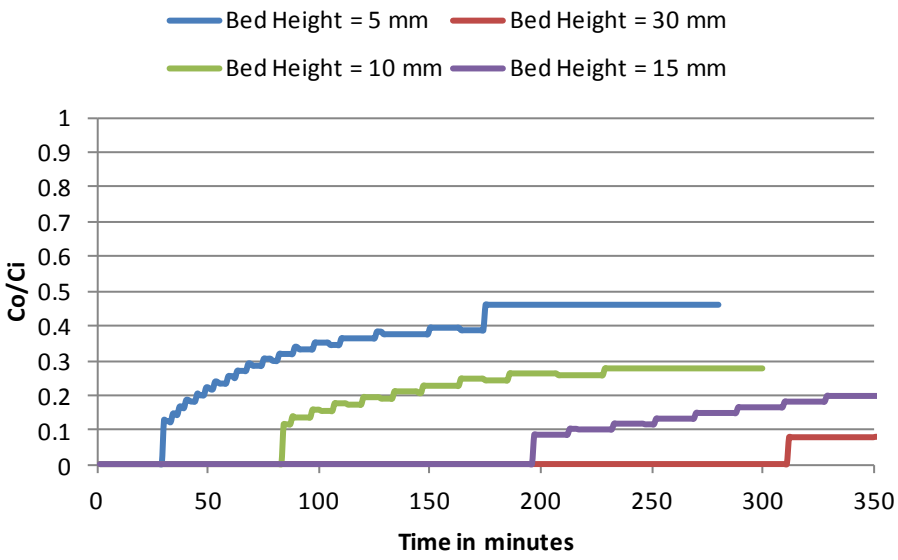

Figure 5-15 Breakthrough curve of Ammonia over Norit RZN01

5.4.2 Norit Vapure 410

Norit Vapure 410, a pelletized form of activated carbon was tested for four packed bed lengths of 20, 30 , 40 and 50mm. 50ppm ammonia gas was supplied from the tank into the packed bed and the breakthrough times were obtained for 11, 39, 60 and 82 minutes. There is an increasing trend

towards equilibrium between phases over time. Similar to RZN01 complete equilibrium was not observed within the time designed for the experiments.

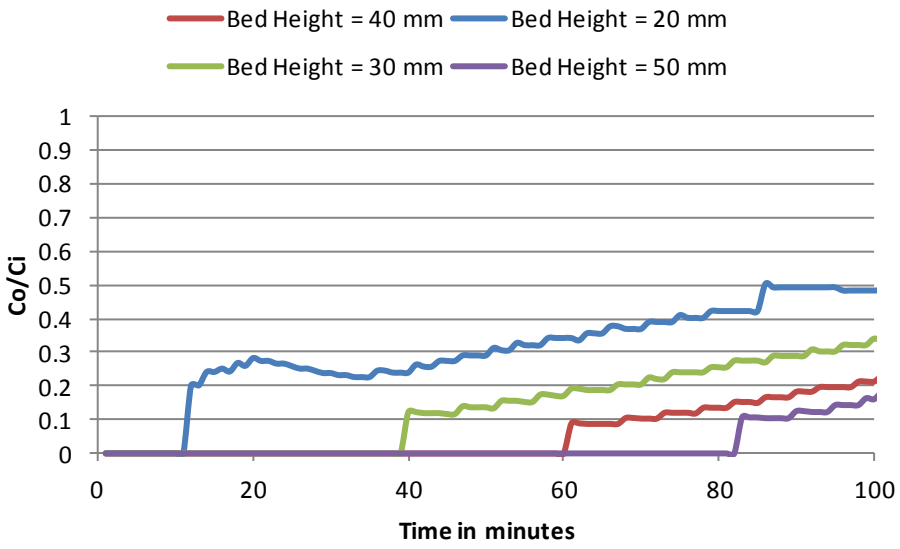

Figure 5-16 Breakthrough curves of Ammonia for Norit Vapure 410

5.4.3 NanoActive MgO

NanoActive MgO is commercially available in powder form, this was loaded into the test facility on a silica matrix to hold the powder and let through the gas. Since this is a powdered form of material, a small orifice was made in the inlet channel and covered with a Teflon tape that acts a pressure relief inside the flow. This will also ensure that the morphologies of MgO are not affected due to the stronger forces per unit area. The flow rates used for these tests were very small approx to 0.51 L/min. Experiments were run for 10, 20, 30 and 35mm of bed lengths and the breakthrough times observed for each flow rate were 168, 200, 227 and 241 minutes respectively.

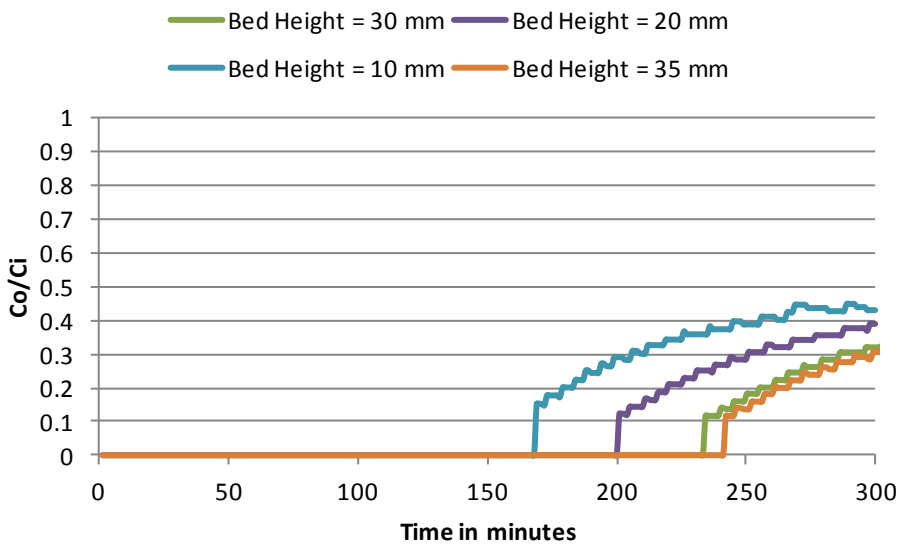

Figure 5-17 Breakthrough curves of Ammonia for NanoActive MgO

5.4.4 NanoActive MgO-G

Granular form of NanoActive MgO was subjected to flow rates of 0.25 L/min for bed heights of 10, 17, 35 and 45 mm. For these tests attainment of equilibrium was clearly seen immediately after the breakthrough of the gas. Time to breakthrough from the results was noted down to be 233, 439, 517 and 556 minutes respectively. The curves obtained are as shown in Figure 5-20.

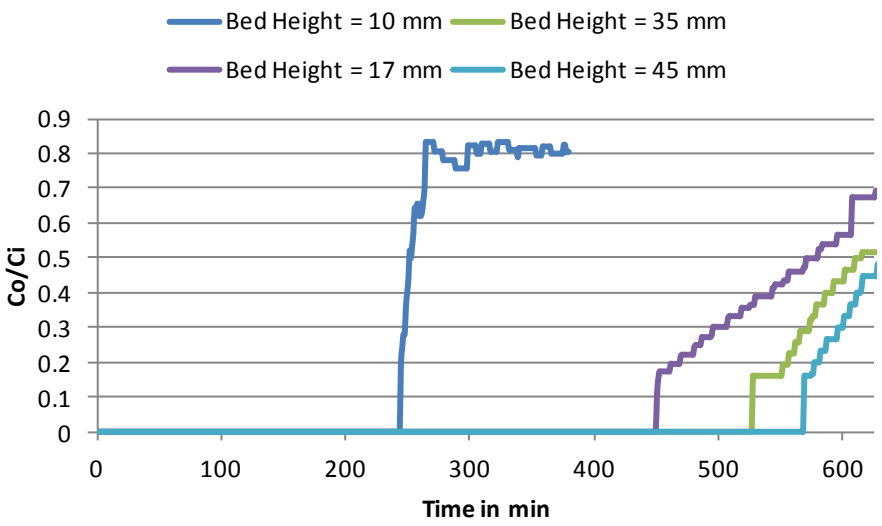

Figure 5-18 Breakthrough Curves of ammonia for Nanoactive™-G MgO

5.4.5 Nanozorb

Nanozorb was tested for breakthrough with 50 mm bed length at 1.2 SCFH flow rate for 6 hours, there was no change in the effluent concentration over the time period. To accelerate the runs, tests were conducted at reduced length of the beds (13mm, 8mm) and varied flow rates of 0.409 L/min and 0.25 L/min. The least bed length (8mm) with a flow rate of 0.25 L/min yielded no breakthrough over a time period of 50 hours.

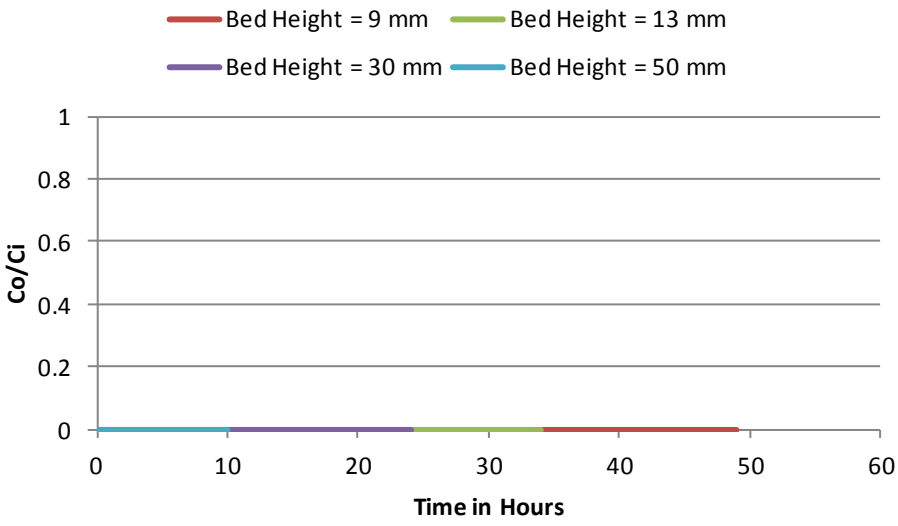

Figure 5-19 Breakthrough test of ammonia for Nanozorb

5.5 Adsorption Capacity

Amount of adsorbent in the bed either in terms of mass or volume of the material is plotted on the abscissa versus time to 5% breakthrough. If a linear relationship is obtained the coefficients of regression equation are used in the estimation of Adsorption capacity and rate constant. From the mass variable breakthrough curves obtained from experiments, breakthrough time as a function of Amount of adsorbent is plotted as shown in Figure 5-22. Polynomial of the form $t_b = a + bW$ was obtained from linear regression analysis.

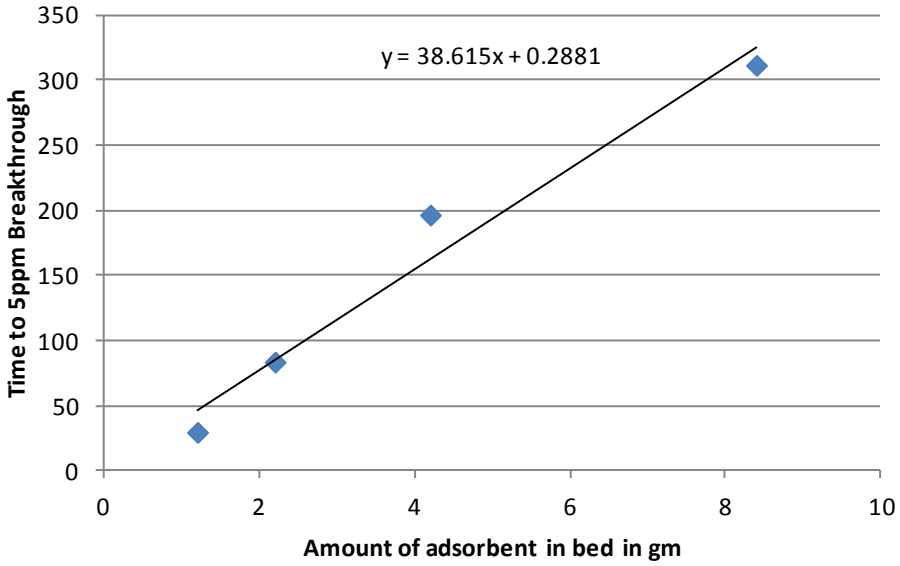

Figure 5-20 Time to breakthrough versus Amount of RZN01

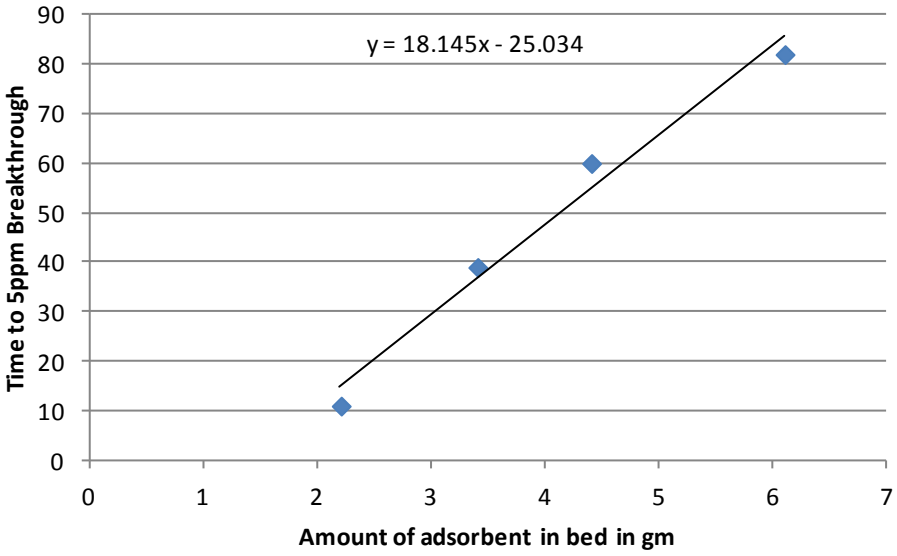

Figure 5-21 Breakthrough time versus Amount of Vapure 410

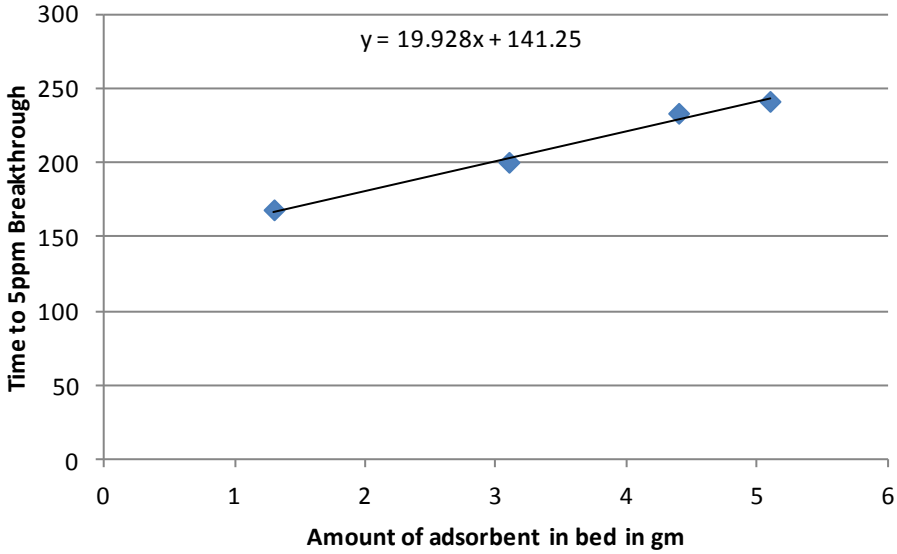

Figure 5-22 Breakthrough time versus Amount of NanoActive™ MgO

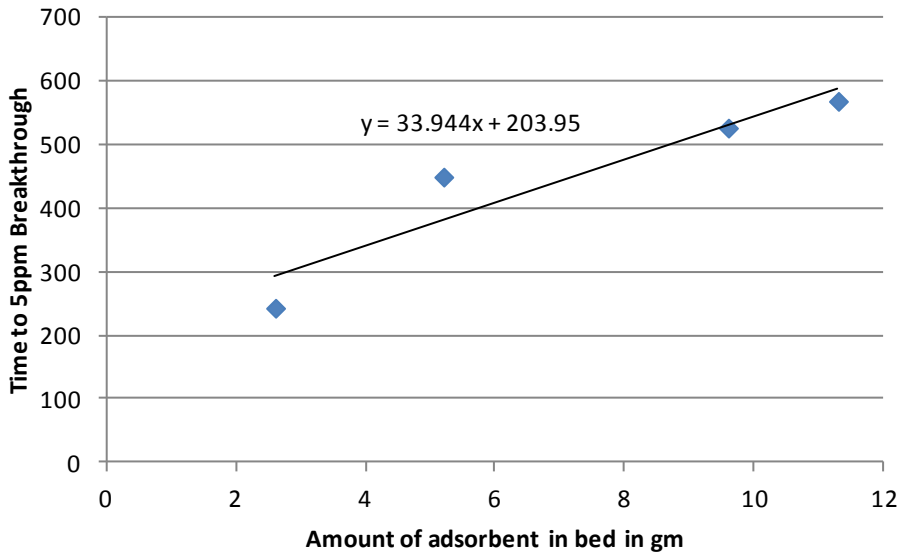

Figure 5-23 Breakthrough time versus amount of NanoActive^{TM}-G MgO

Four adsorbents out of six tested for BTC's are plotted for regression analysis. The plots above Figure 5-22, Figure 5-23, Figure 5-24, Figure 5-25 show the time to breakthrough for a specified concentration 5ppm of adsorbate gas against the amount of carbon in the bed. The variable for each dynamic contour is length of the bed or in other terms the volume of the bed for a fixed column. The amount of carbon is expressed in terms of mass(g) and volume (cm^3). RB 40M did not show any signs of breakthrough and the trend was rather unusual from conventional curves. On the other hand NanoZorb worked very well but there was no rise in the BTC, which is required for the estimation of fractional breakthrough point. Hence these two materials are excluded from further calculations. A good linear regression fit can be seen for RZN01, Vapure 410, NanoActive^{TM} MgO and NanoAcitve^{TM}-G MgO respectively. The coefficients obtained are shown in Table 5-5.

Table 5-5 Coefficients of Regression Equation $t_b = a + bW$, and the correlation data coefficient

Adsorbent	a	b	R^2
RZN01	0.28	38.61	0.9655
Vapure 410	-25.03	18.14	0.9779
NanoActive MgO	141.25	19.92	0.991
NanoActive MgO-G	203.95	33.94	0.8798

Examination of modified Wheeler equation shows that

$$\boldsymbol{a} = -\boldsymbol{W_e \rho_B} \, \boldsymbol{ln} \frac{\left(\frac{\boldsymbol{C_i}}{\boldsymbol{C_o}}\right)}{\boldsymbol{C_i k_v}} \tag{5.8}$$

$$\boldsymbol{b} = \frac{\boldsymbol{W_e}}{\boldsymbol{C_o Q}} \tag{5.9}$$

From known values of C_o and Q, the kinetic/dynamic adsorption capacity, W_e can be determined from Equation (5.6). The dynamic adsorption capacity of the novel materials for the Ammonia gas under the conditions of the test W_e, by fitting the data to the wheeler equation as modified by Jonas and coworkers, data taken from the linear regression curves are used to illustrate the calculation.

From the modified Wheeler equation/Wheeler-Jonas equation, the slope of the breakthrough time versus carbon volume plot is equal to the following:

$$\frac{W_e}{C_o Q}$$

Where C_o = inlet concentration of adsorbate in g/cm^3.

5.6 Surface Area, Pore Volume and Adsorption capacity

Table 5-6 lists the properties of all the adsorbents. Adsorption capacity is defined with units, gm of adsorbate (NH_3) per unit volume (cubic centimeter) of adsorbent.

Table 5-6 Comparison of Adsorption capacity and Surface area

Material	Adsorption Capacity(gm of NH_3/cc of Adsorbent)	BET Surface Area (m^2/g)	Pore Volume(cm^3/g)
Norit RZN01	2.02E+00	4.60E+02	8.81E-02
Norit Vapure 410	9.60E-01	9.01E+02	2.36E-01
Norit RB 40M	n/a	8.10E+02	0.196
NanoActive™ MgO	1.06E+00	2.42E+02	3.24E-01
NanoActive™-G MgO	1.81E+00	n/a	n/a
NanoZorb®	n/a	n/a	n/a

The adsorption capacities of novel materials for ammonia are compared with the carbon based materials for the adsorption of di methyl ether from ASTM standard D5160 [27]. The materials from Table 5-7 show values for the adsorption properties when activated carbon is enhanced with carbon tetra chloride activity (CTA) produced from coconut and charcoal.

Table 5-7 Comparison of Adsorption capacity with literature

Material	Adsorption Capacity(gm of NH_3/cc of Adsorbent)	Material	Adsorption Capacity(g di methyl ether/cc of adsorbent)
Norit RZN01	2.02E+00	12x20 mesh coconut CTA 57.9%	1.30E-02
Norit Vapure 410	9.60E-01	12x20 mesh coconut CTA 70.3%	7.94E-03
NanoActive™ MgO	1.06E+00	12x30 mesh coal CTA 76%	5.91E-03
NanoActive™-G MgO	1.81E+00	12x30 mesh coconut CTA 102%	4.67E-03

5.7 Rate Coefficients and Effectiveness Factors

Adsorption rate constant k_v was calculated for each material listed in Table5-7, inserting into it the square root of known molecular weight for the vapor. The obtained rate constants are compared with pore size of the materials.

Table 5-8 Comparison Adsorption Rate constants for the Adsorbents against Ammonia with pore size

Material	K_v (1/min)	Pore size in Å
Norit RZN01	2.00E+05	17.66
Norit Vapure 410	1.19E+03	16.85
NanoActive™ MgO	2.96E+02	27.13
NanoActive™-G MgO	6.55E+02	n/a
Norit RB 40M	n/a	17.06

Adsorption rate from the experiments is compared with theoretical models developed by Wood and Nelson (Appendix A.2.3). There is a good agreement between theoretical and experimental values of rate constant as shown in Table 5-8. NanoActive™ MgO has considerable deviation from theoretical rate constant. The values are plotted on graph as shown in Figure 5-26. Since the scale range is wide on the y-axis, log-graph is plotted to observe the deviation between experimental k_v and theoretical k_v as shown in Figure 5-27. k_v theoretical is calculated from Equation (5.7)

$$\boldsymbol{k} = \frac{\boldsymbol{48\beta^{0.33} v_L^{0.75}}}{\boldsymbol{d_p^{1.5}}} \tag{5.10}$$

Table 5-9 Experimental and calculated values of k_v

Material	k_v Experimental (1/min)	k_v Theoretical (1/min)
Norit RZN01	2.00E+05	1.92E+05
Norit Vapure 410	1190	1348
NanoActive™ MgO	2.96E+02	16.3E+06
NanoActive™-G MgO	6.55E+02	1034

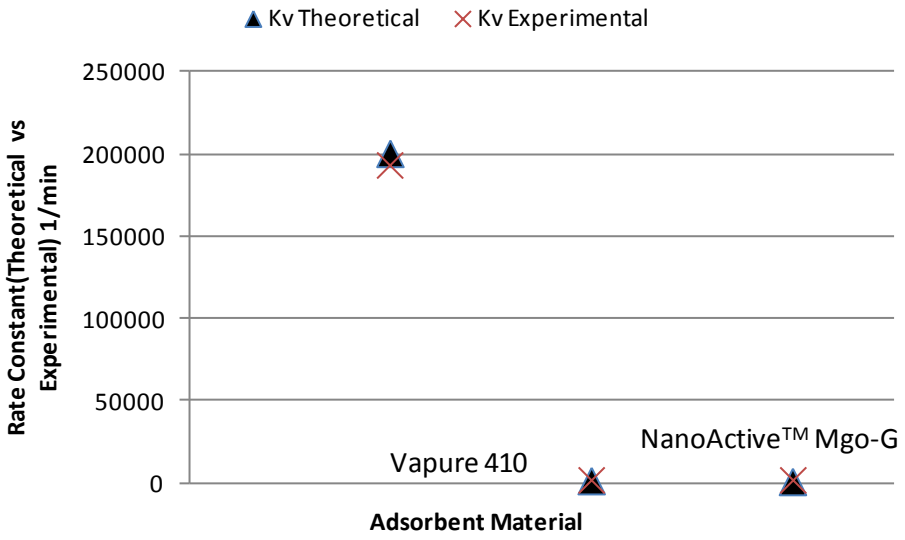

Figure 5-24 Experimental versus theoretical rate constant

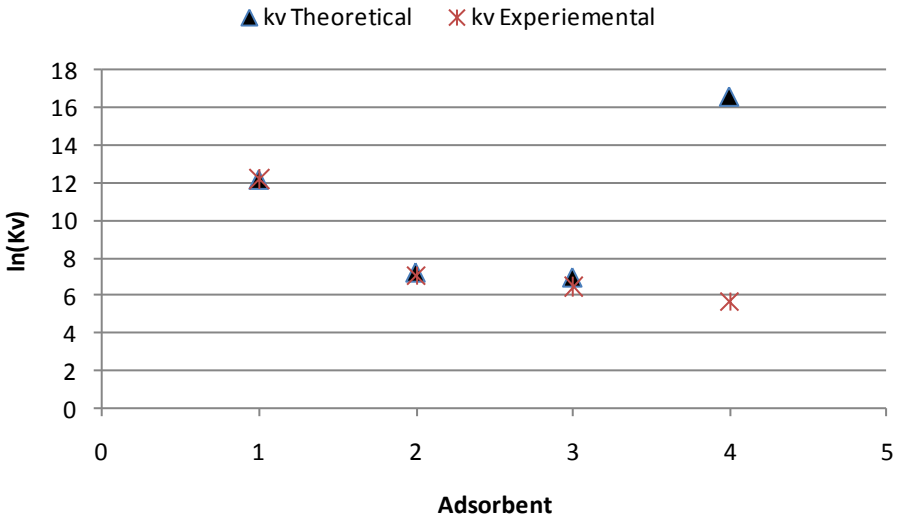

Figure 5-25 Log plot comparison of experimental and theoretical rate constants

Effectiveness factors for each adsorbent and its effect on mass as variable is plotted. Effectiveness factor is given by [15]

$$e_R = A_1 \frac{QC_i}{(q_o.W + \varepsilon_L.V.C_i)} \tag{5.11}$$

Parameters for equation (5.8) are discussed in Appendix A.2.4. For the study of effectiveness factor, the values were calculated at 10% cut off (10% of C_0/C_i). Effectiveness factor for Norit based carbonaceous compounds increased with increasing amount of material. The maximum amount of adsorbate was relatively lower than the actual amount present in the column, thus the equilibrium was attained faster for the Norit materials. Whereas, the NanoActive™ materials showed a linearly decreasing trend with increasing mass of adsorbent which indicates weak driving forces along the pores compared to Norit materials.

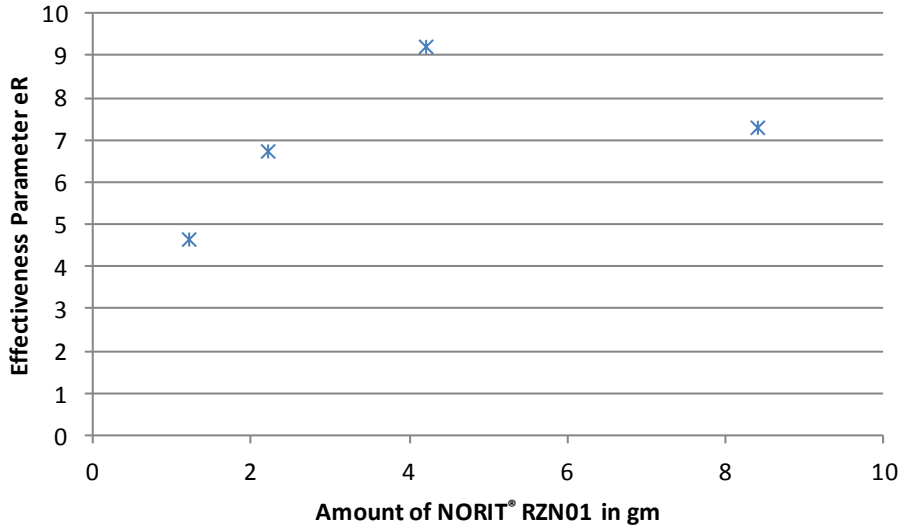

Figure 5-26 Effect of amount of RZN01 on effectiveness factor

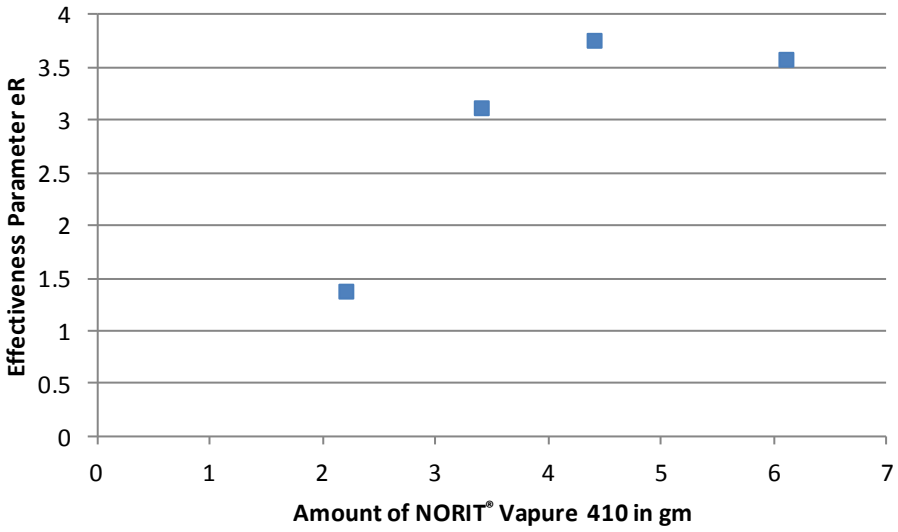

Figure 5-27 Effect of amount of Vapure 410 on effectiveness factor

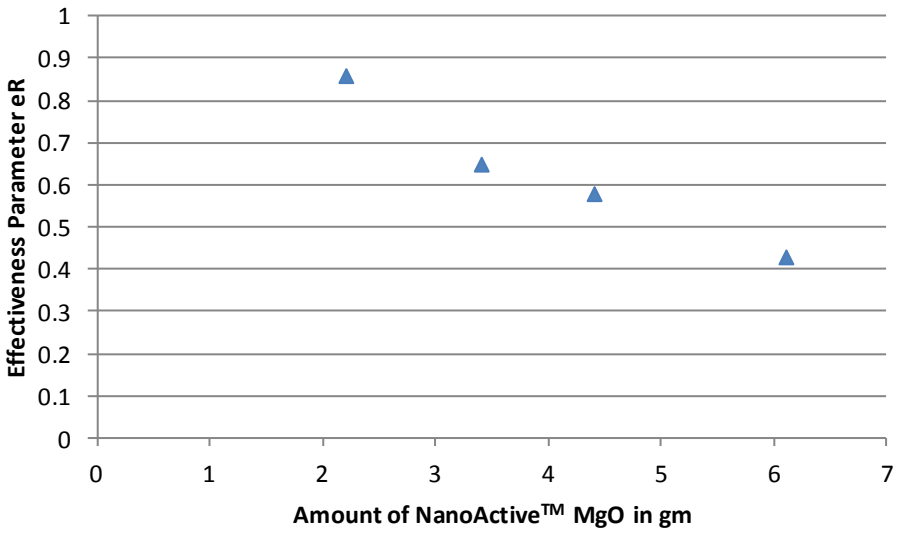

Figure 5-28 Effect of amount of NanoActive™ MgO on effectiveness factor

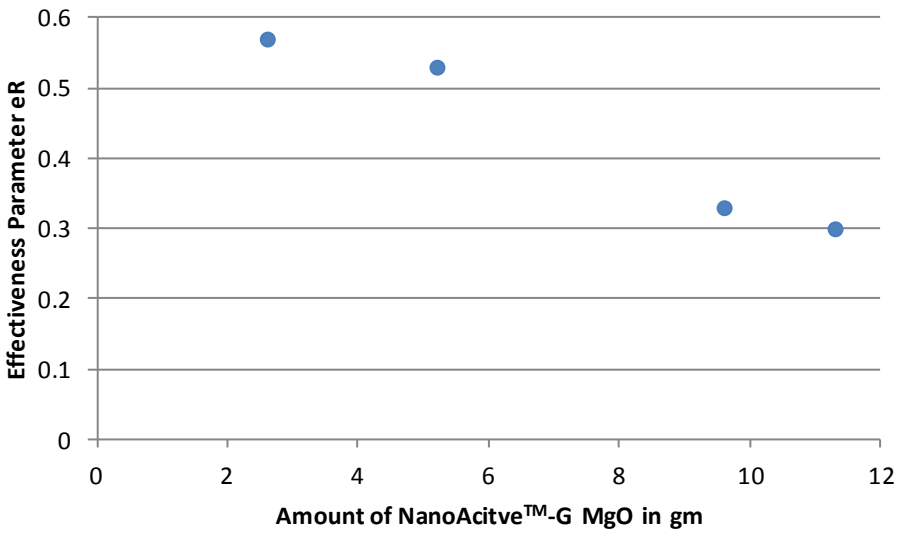

Figure 5-29 Effect of amount of NanoActive™-G MgO on effectiveness factor

Correlations between pressure drop and flow rates were established for two discrete shaped, cylindrical and spherical packed beds. Surface areas of the novel materials are measured in BET tester and their pore volumes are compared. Breakthrough curves for two different variables are performed using the test facility designed for nanomaterials. The final breakthrough curves with flow rate as a variable indicate that NanoActive™ materials have adsorption capacities of 1.81 and 1.06 compared to capacity of 2.01 for research grade doped carbon compounds. BTC curves obtained for variable amount of material show a delayed response to achieve steady state, indicating slow adsorption kinetics through the bed. The effectiveness factor in the range of 0.3 and 0.9 indicates existence of weak interactions between the gas phase and solid phase for NanoActive™ materials.

Chapter 6 - Conclusion

Pressure drop is measured as a function of flow rate for flow in packed beds. Two different primary shapes of particles, cylindrical and spherical were tested for energy losses in fixed bed column. Pressure drop and flow rate data is converted into Reynolds number and Friction factor and compared with Ergun equation. The correlations were compared with Ergun data for cylindrical pellets and Idlechik method for spherical spheres. Dependence of pressure drop/Length on flow rates and its variation with Volume fraction of pellets is identified. Volume/solid fractions of 0.4±0.02 were used to identify the sustainability of the packed bed.

NanoActive^{TM} MgO has obtained a low value of surface area ($2.4x10^2$ m^2/g), using the nitrogen adsorption technique. Whereas Norit based materials obtained comparatively higher surface areas (460 m^2/g, 910 m^2/g) for the same test.

Breakthrough curves for 6 different materials were produced using the test facility-2 embedded with gas detectors. The curves obtained are utilized to draw the curves between 5% breakthrough against the amount of adsorbent in the bed. Adsorption capacities were calculated when a linear relationship is found. The best adsorbent for ammonia adsorption should have the highest dynamic adsorption capacity coupled with short mass transfer zone. Norit based RZN01 had the highest adsorption capacity of 2.02 g of NH_3/cc of RZN01. In NanoActive^{TM} based materials NanoActive^{TM}-G MgO had the highest adsorptivity of 1.81 g of NH_3/cc of MgO-G. Though there isn't much difference between their adsorption capacities, rate constant had a much higher value of 2.00E+05 for Norit RZN01 than any other material. This implies the gas-solid interaction kinetics is more rapid in Norit RZN01compared to other materials. Norit RZN01 was originally designed (cylindrical pellets) for ammonia removal; the functional groups that would enhance adsorption were present in the adsorbent. This is not the case with NanoActive^{TM} materials; they were purchased commercially and tested without tampering chemical and physical properties. These are interesting results since the adsorption capacity of NanoActive^{TM} materials were almost equivalent to the values obtained for Norit based research grade materials, though their surface areas were relatively low.

Effectiveness factors were evaluated for both Norit and NanoActive materials, driving forces were weak in NanoActive powders and pellets (granular) compared to norit materials. These results are indicative of the fact that metal oxide nanoparticles need to be doped with

ammonia removal ligands for enhancement affinity of retention. In addition Magnesium Oxide reacts readily with water and the relative humidity may also affect the effectiveness of interaction.

NanoZorb® didn't express any change in the exit concentration for prolonged measurements of time. The same behavior was observed for repeated number of times, there was no change in the response of the curves even for increased flow rates. From the experimental data it is logical to conclude NanoZorb® possess a very high adsorption capacity for the adsorption of Ammonia. There is a scope for further investigation to uncover the full potential of NanoZorb® as an adsorbent.

References

1. Ergun, Sabri, "Fluid Flow through Randomly Packed Columns and Fluidized Beds." *Industrial and Engineering Chemistry,* Vol. 41, No. 6 (1949): 1179-1184
2. Kenneth J. Klabunde, Jane Stark, Olga Koper, Cathy Mohs, Dong G. Park,1 Shawn Decker, Yan Jiang, Isabelle Lagadic, and Dajie Zhang (*J. Phys. Chem.* 1996). Nanocrystals as Stoichiometric Reagents with Unique Surface Chemistry, *100,* 12142-12153
3. The Adsorption of Gases and Vapors, Volume 1 Physical Adsorption by Stephen Brunauer
4. The Solid-Gas Interface Volume 1 Edited by E. Alison Ford
5. Eric B Sansone, Yadu B Tewari and Leonard A Jonas," Prediction of Removal of Vapors from Air by Adsorption on Activated Carbon" (December 1979) *American Chemical Society Volume 13, Number 12*
6. www.epa.gov/apti/Materials/APTI%20415%20student/415%20Student%20Manual/415_Chapter_4_12-15-2008
7. Wheeler, A., Robell, A.J., *Journal of Catalysis.,* (1969) Performance of fixed-bed catalytic reactors with poison in the feed 13, 299-305
8. L.A. Jonas, and J.A. Rehrmann, The kinetics of adsorption of organo-phosphorous vapors from air mixtures by activated carbons, Carbon 10, 657-663, 1972
9. Gerry O Wood and P.Lodewyckx, An extended equation of rate coefficients for adsorption of organic vapors and gases on activated carbons in air-purifying respirator cartridges. American Industrial Hygiene Association Journal 64:646-50.2003
10. K.D. Henning, S.Schafer, Impregnated activated carbon for environmental protection, *Gas separation and Purification Journal* 1993; 7(4):235-240
11. L. Verhoeven and P. Lodewyckx Using the Wheeler-Jonas equation to describe adsorption of inorganic molecules: Ammonia, *Proceedings of the Second International Carbon Conference, Lexington, KY, USA*; 2001

12. Soo-Jin Park , Byung-Joo Kim (Journal of Colloid and Interface Science 291 (2005)Ammonia removal of activated carbon fibers produced by oxyfluorination 597–599
13. Sridhar,P., N.V.S. Sastri, J.M. Modak, and A.K. Mukherjee, "Mathematical Simulation of Bioseperation in an Affinity Packed Column," Chem. Eng. Technol.,17, 422(1994)
14. Niemeyer, B., T.Feilenreiter, and H.Tiltscher, "Theoretical Studies on Biospecific Adsorption of Large-Scale Affinity Separations," Chem. Eng. Sci., 51(24), 5263 (1996)
15. L. F. Bautista, M. Martınez,and J. Aracil, Adsorption of α-Amylase in a Fixed Bed: Operating Efficiency and Kinetic Modeling (*AIChE Journal October 2003*) *Vol.49, No.10*
16. A. Srivastava, O. N. Srivastava, S. Talapatra, R.Vajtai and P. M. Ajayan (August 2004) Carbon nanotube filters *doi:10.1038/nmat1192*
17. Christian L. Mangun, Richard D. Braatz, James Economy, and Allen J. Hall, (*Ind. Eng. Chem. Res.* 1999) Fixed Bed Adsorption of Acetone and Ammonia onto Oxidized Activated Carbon Fibers, *38,* 3499-3504
18. Stephan brosillon, marie-helenemanero and jean-noelfoussard (*Environ. Sci. Technol*. 2001), Mass Transfer in VOC Adsorption on Zeolite: Experimental and Theoretical Breakthrough Curves 35, 3571-3575
19. http://www.nanoscalecorp.com/resources/Literature/NanoActive_Magnesium_Oxide.pdf
20. http://www.norit-americas.com/resources/technical-datasheets.php
21. Gerry O. Wood and Ernest S. Moyer, A Review of the Wheeler Equation and Comparison of its Applications to Organic Vapor Respirator Cartridge Breakthrough Data(American Industrial Hygiene Association Journal) Vol.50, Issue 8, 1989, *doi: 10.1080/15298668991374886*
22. P.Lodewyckx, Teresa Valdés-Solís, Marco J.G.Linders and Freek Kaptejin, Application of the wheeler-jonas equation for the calculation of carbon monolith breakthrough times *Int.Carbon Conference, Providence RI (USA)*, 2004
23. Jonas L.A., Tewari Y.B., Sansone E.B., Carbon, in press.
24. Ergun, Sabri, "Fluid Flow through Packed Columns." Chemical Engineering Progress, Vol 48, No2. (1952): 89-84

25. Dubinin, M.M., *Progress in Surface and Membrane Science*., 9, 1-70 (1975)
26. Fried Erwin, Idlechik, I.E, “Flow resistance: A design guide for engineers”, Book (ISBN 0891164359), 1989
27. Standard Guide for Gas-Phase Adsorption Testing of Activated Carbon, ASTM standard D5160-95 (Reapproved 2008)

Appendix A - Supplemental Data

A.1 Calibration Curves

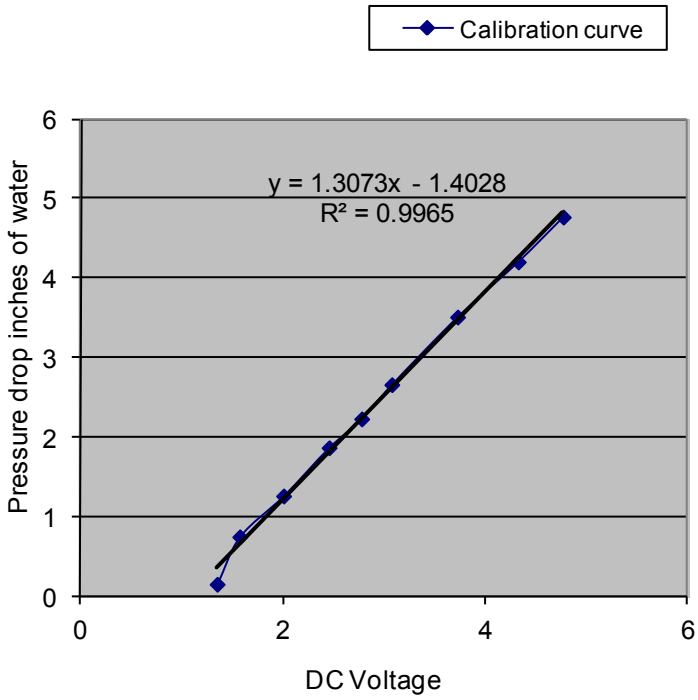

Figure A-1 Calibration curve of pressure transducer with standard ethyl alcohol in manometer

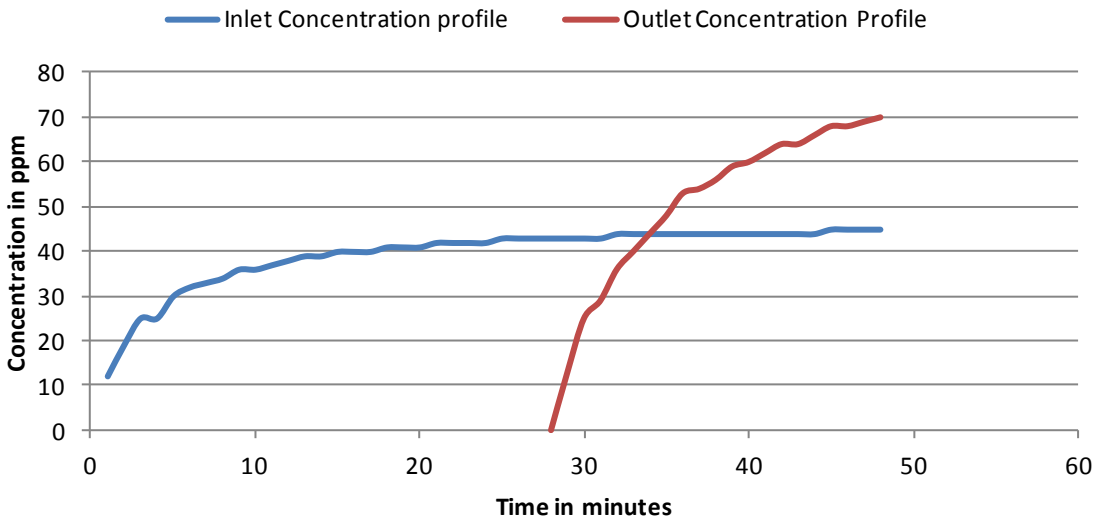

Figure A-2 Concentration profile pre-calibration of Altair-5 gas monitors

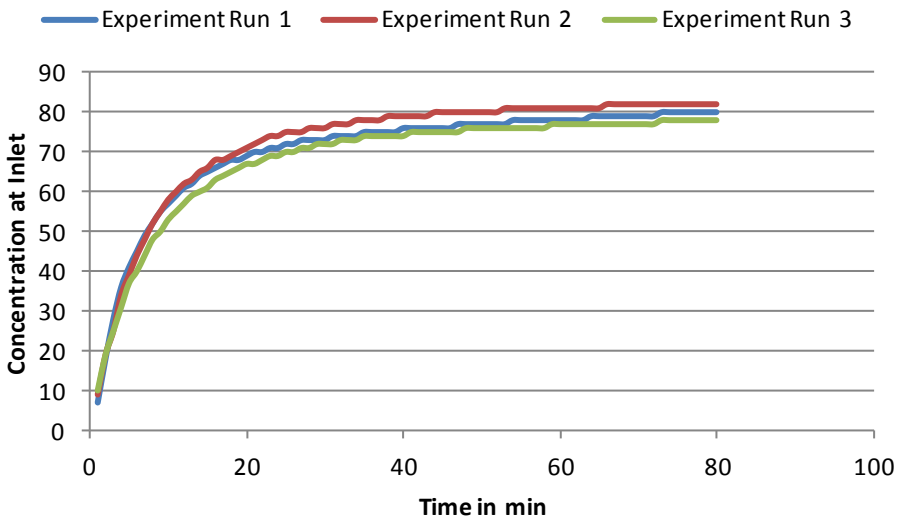

Figure A-3 Concentration profiles post-calibration of Altair-5 gas monitor at column inlet

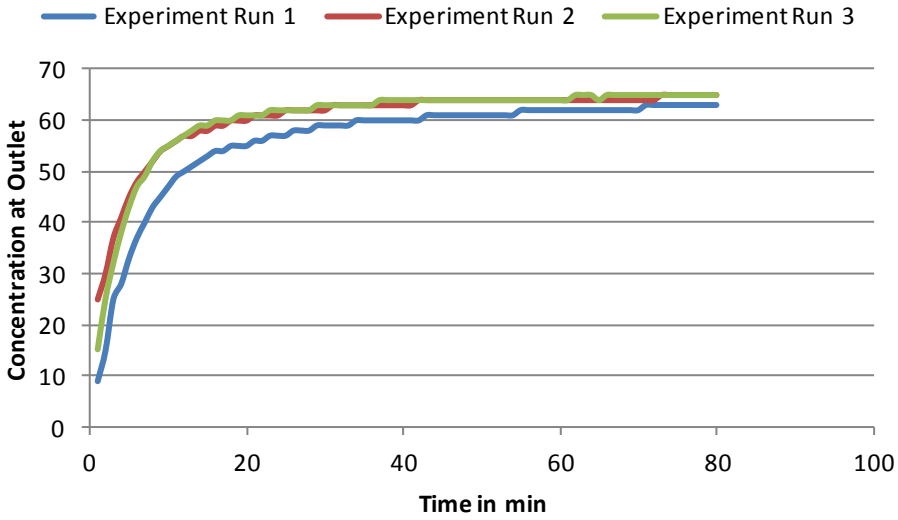

Figure A-4 Concentration profile post-calibration of Altair-5 monitor at column outlet

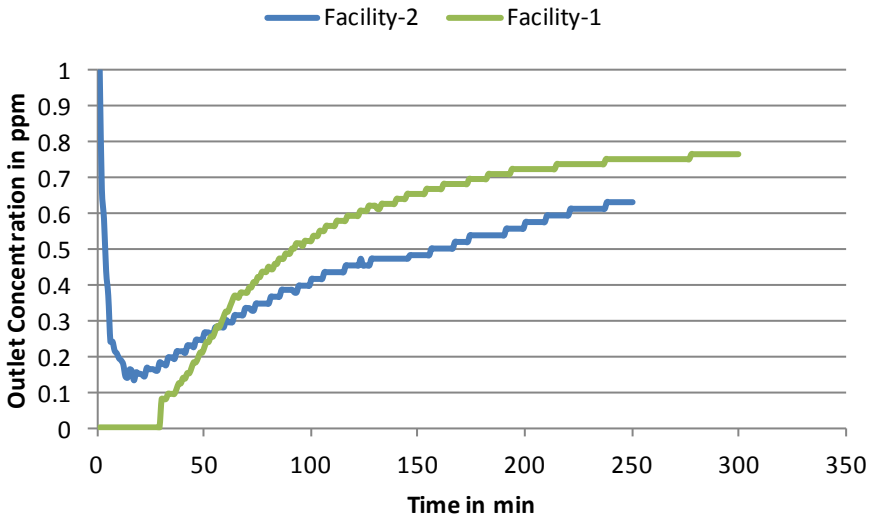

Figure A-5 Outlet concentration profile comparison of both facilities in similar conditions

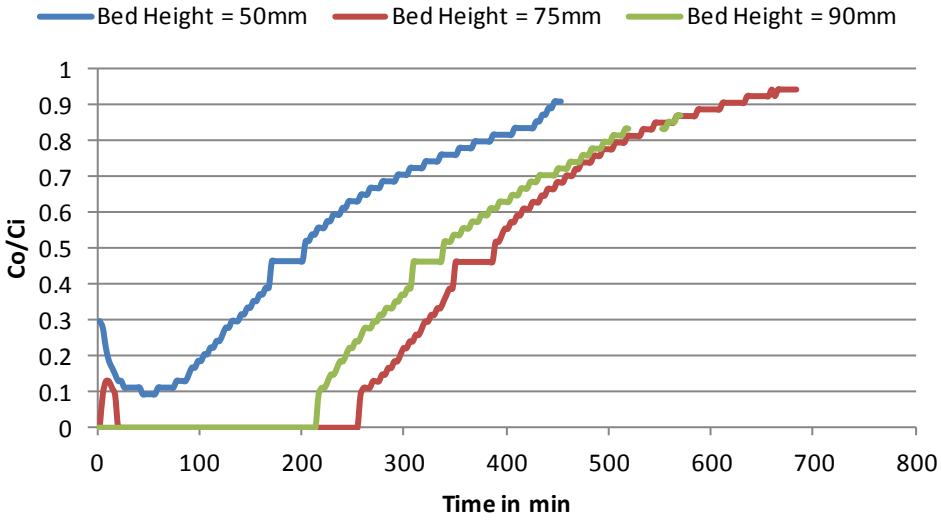

Figure A-6 Breakthrough curves for the adsorption of ammonia on low grade activated carbon in facility-1

A.2 Calculations

A.2.1 Conversion of SCFH to CFH

Using Charles law, at constant pressure, the volume of a gas is directly proportional to the absolute temperature. Standard conditions are 491.67°R at 14.696 psi and the room conditions are 534.87°R (24°C)

$$\frac{V_{STD}}{V_{ACT}} = \frac{T_{STD}}{T_{ACT}}$$

Table A-1 Converted flow rate values from SCFH to CFH

Flow rate in SCFH	Flow rate in CFH
0.8	0.87
1	1.08
2	2.1
3	3.28
4	4.35
5	5.4
6	6.48
7	7.56
8	8.64
9	9.72
10	10.8
11	11.88
12	12.96

A.2.2 Sutherlands Conversion

At 15°C μair = 1.78 x 10^{-5} kg/ms, T_o=524°R, μ_o=0.01827 cP (centi poise)

$$a = 0.555(T_o) + C$$

$$b = 0.555(T) + C$$

Sutherlands Formula, Viscosity of air at experimental conditions

$$\mu = \mu_o \left(\frac{a}{b}\right)\left(\frac{T}{T_o}\right)^{\frac{3}{2}}$$

$$\mu = 1.85 \times 10^{-5}\text{kg/ms}$$

Table A-2 Friction factors for varied column heights of activated carbon pellets

Flow rate in SCFH	Reynolds Number	Superficial Velocity m/s	F_{p1}	F_{P2}	F_{P3}	F_{P4}
12	140.95	0.3229	17.74	6.49	3.31	2.57
11	129.02	0.3047	19.73	7.29	3.74	2.87
10	112.77	0.2663	24.09	8.98	4.64	3.47
9	105.73	0.2497	25.46	9.55	4.95	3.68
8	93.79	0.2215	29.75	11.28	5.87	4.3
7	81.69	0.1929	36.72	13.92	7.31	5.3
6	70.28	0.166	48.42	18.45	9.64	6.96
5	58.52	0.1382	66.95	25.63	13.46	9.62
4	46.44	0.1097	101.47	38.86	20.32	14.47
3	35.2	0.0832	173.8	66.16	35.2	24.6
2	21.17	0.050	470	180	95.8	66.8

A.2.3 Overall Adsorption Rate Coefficient

$$k = \frac{48\beta^{0.33}{v_L}^{0.75}}{{d_p}^{1.5}}$$

$\beta = 0.28$ for Ammonia

v_L is the linear velocity cm/s

d_p mean diameter of the particles cm

Table A-3 Theoretical rate coefficient of adsorbents

Material	Mean diameter d_p cm	v_L, cm/s	K_v, 1/min
RZN01	0.09	9.06	1.92×10^5
Vapure 410	0.3375	6	1348
NanoActive MgO	0.00003	3	16.3×10^6
NanoActive-G MgO	0.119	1.49	1034.3

A.2.4 Effectiveness factor parameters

V total volume of adsorber (cm^3)

C_i column inlet concentration of the gas phase

q_o*W maximum amount of adsorbate inside the column

ε is the bed porosity

$$\varepsilon = \frac{A}{\left(\frac{D}{d}\right)^n} + B$$

n shape factor

D/d is ratio of Vessel diameter to the grain diameter

Table A-4 Shape factors for standard size particles

Shape of grain	A	B	n
Spheres	1	0.375	2
Cylinders	0.9198	0.3414	2
Irregular Shape	1.5	0.35	1

Table A-5 Average bed porosity of adsorbent bed

ε	Norit RZN01	Vapure 410	NanoActive MgO	NanoActive-G MgO
A	0.9198	1.5	1	1.5
B	0.3414	0.35	0.375	0.35
n	2	1	2	1
D/d	211.1	9.5	6333	15.96
ε	0.34	0.5	0.375	0.44